

# Generalized Normalizing Flows via Markov Chains

Paul Lyonel Hagemann\*    Johannes Hertrich\*    Gabriele Steidl\*

February 7, 2022

Normalizing flows, diffusion normalizing flows and variational autoencoders are powerful generative models. This chapter provides a unified framework to handle these approaches via Markov chains. We consider stochastic normalizing flows as a pair of Markov chains fulfilling some properties and show how many state-of-the-art models for data generation fit into this framework. Indeed including stochastic layers improves the expressivity of the network and allows for generating multimodal distributions from unimodal ones. The Markov chains point of view enables us to couple both deterministic layers as invertible neural networks and stochastic layers as Metropolis-Hastings layers, Langevin layers, variational autoencoders and diffusion normalizing flows in a mathematically sound way. Our framework establishes a useful mathematical tool to combine the various approaches.

## 1. Introduction

Deep generative models for approximating complicated and often high-dimensional probability distributions became a rapidly developing research field. Variational autoencoders (VAEs) were originally introduced in [38] and have seen a large number of modifications and improvements for quite different applications. For some overview on VAEs, we refer to [39]. Recently, diffusion normalizing flows arising from the Euler discretization of a certain stochastic differential equation were proposed in [65]. On the other hand, normalizing flows including invertible residual neural networks (ResNets) considered in [6, 8, 28], invertible neural networks, see, e.g., [4, 15, 25, 37, 44, 50] and autoregressive flows examined in [13, 16, 34, 47] are a popular classes of generative models. In this tutorial, we are interested in finite normalizing flows which are basically concatenations of diffeomorphisms with tractable Jacobian determinant. For their continuous counterpart we refer to the overview paper [53] and the references therein.

Unfortunately, invertible neural networks suffer from a limited expressiveness. More precisely, their major drawbacks are topological constraints, see, e.g. [18, 19]. For example, when trying to map a unimodal (latent) distribution to a multimodal (target) distribution, connections between

---

\*TU Berlin, Straße des 17. Juni 136, D-10623 Berlin, Germany, {hagemann,j.hertrich,steidl}@math.tu-berlin.de.

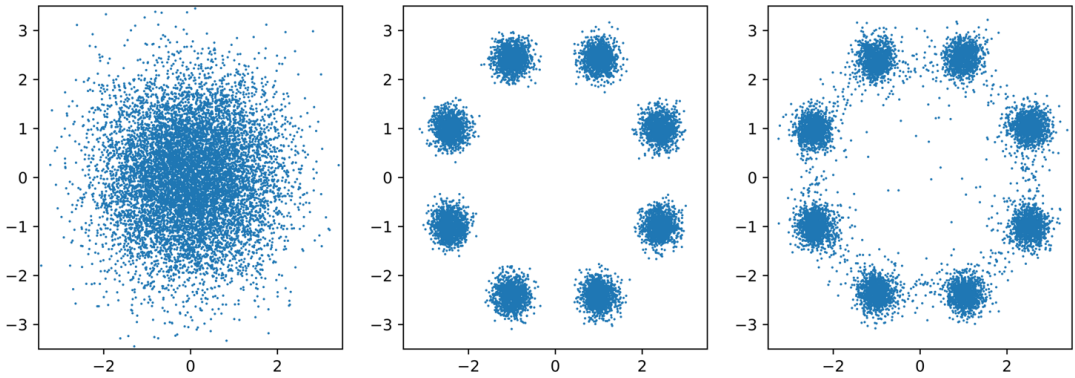


Figure 1.1: Lack of expressiveness of invertible neural network. Left: Gaussian standard distribution (latent distribution), Middle: Gaussian mixture distribution with colors (target distribution), Right: Results of an invertible neural network trying to generate the multimodal distribution from the unimodal Gaussian one.

the modes remain. It was shown in [25], see also [7, 10], that for an accurate match between such distributions, the Lipschitz constant of the inverse flow has to approach infinity. Similar difficulties appear when mapping to heavy-tailed distributions as observed in [36]. See Figure 1.1 for a typical example.

To overcome topological constraints and improve the expressiveness of normalizing flow architectures, the authors of [64] introduced stochastic normalizing flows which combine deterministic, learnable flow transformations with stochastic sampling methods. One way to think about those stochastic sampling methods is that they force the flow to obey a certain path: Often, for MCMC or Langevin methods, one needs to specify a density to anneal to, so that we define a path on which the flow moves to the target density. The advantages can be seen in Figure 1.2. Here on the left there is the modeled density of an image as a 2d density with stochastic normalizing flow versus a standard invertible neural network on the right. The stochastic steps enable to model high concentration regions much better without smearing leaving connections between modes. However, it turns out that also variational autoencoder can be modeled as stochastic layers. For those layers, we do not need to define interpolating densities, we only need to relax our notion of invertibility to "probabilistic" invertibility.

In [24] we considered stochastic normalizing flows from a Markov chain point of view. In particular, we replaced the transition densities by general Markov kernels and provided mathematically sound derivations using Radon-Nikodym derivatives. This allowed to incorporate deterministic flows as well as Metropolis-Hastings flows which do not have densities into the mathematical framework.

The aim of this tutorial is to propose the straightforward and clear framework of Markov chains to combine *deterministic* normalizing and *stochastic* flows, in particular VAEs, diffusion normalizing flows and MCMC layers.

More precisely, we establish a pair of Markov chains that are inverse to each other in a broad

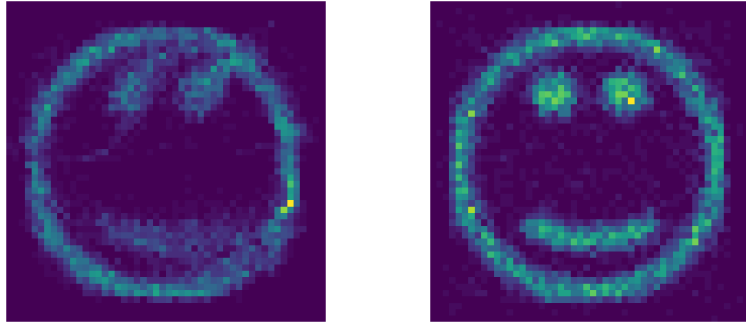


Figure 1.2: Lack of expressiveness of normalizing flows as opposed to stochastic normalizing flows. A smiley modeled as 2d density generated by a normalizing flow on the left and with stochastic steps on the right.

sense we will explain later. This provides a powerful tool for coupling different architectures, which are used in many places in the machine learning literature. However, viewing them through the lens of stochastic normalizing flows a lot of very recent ideas can be *unified* and *subsumed* under this notion, which is quite elegant and useful. This gives a tool to combine variational autoencoder, diffusion layers which are inspired by stochastic differential equations, coupling based invertible neural network layer and stochastic MCMC methods all in one. Furthermore, we will provide a loss function that is an upper bound to the Kullback–Leibler distance between target and sampled distribution, enabling *simultaneous* training of all those layers in a data driven fashion. We will demonstrate the universality of this framework by applying this to three inverse problems. The inverse problems consist of conditional image generation via 2d densities, a high-dimensional mixture problem with analytical ground truth and a real world problem coming from physics.

## Related work

Among the first papers which introduced stochastic diffusion like steps for forward and backward training of Markov kernels was [54]. Further, stochastic normalizing flows are closely related to the so-called nonequilibrium candidate Monte Carlo method from nonequilibrium statistical mechanics introduced in [46]. Here, the authors constructed a MCMC method by generating a sequence  $(x_n)_n$  in the following two steps: first, based on the point  $x_n$ , they construct a candidate  $x'$  by a sequence of deterministic flow transformations and stochastic sampling methods. Second, they either accept or reject the point  $x'$ . If  $x'$  is accepted, then  $x_{n+1} := x'$ . Otherwise,  $x_{n+1}$  is set to a point  $\tilde{x}'$  generated by the so-called momentum reversed transformations of  $x'$ . The first of these steps is very similar to SNFs with the difference that the deterministic flow transformations are not learned, but given by a certain application. Furthermore, the authros of [3] propose the use of importance sampling and MCMC kernels in conjunction with normalizing flows, but in contrast to [64] the layers are learned individually. Relations between normalizing flows and other approaches as VAEs were already mentioned in the literature. So there exist several

works which model the latent distribution of a VAE by normalizing flows, see [12, 50], or by stochastic differential equations see [61]. Using the Markov chain derivation, all of these models can share a lot of similarities with stochastic normalizing flows, even though some of them employ different training techniques for minimizing the loss function. Further, the authors of [23] modified the learning of the covariance matrices of decoder and encoder of a VAE using normalizing flows. This can also be viewed as one-layer stochastic normalizing flow. A similar idea was applied in [42], where the weight distribution of a Bayesian neural network by a normalizing flow was modeled. To bridge the gap between VAEs and flows, the authors of [45] introduce injective and surjective layers and call them SurVAEs. They introduce a variety of layers to make use of special structure of the data, such as permutation invariance as well as categorical values. This paper makes use of similar ideas as stochastic normalizing flows and also implemented variational autoencoder layer within the normalizing flows framework.

Further, to overcome the problem of expensive training in high dimensions, some recent papers as, e.g., [11, 40] propose also other combinations of a dimensionality reduction and normalizing flows. The construction of [11] can be viewed as a variational autoencoder with special structured generator and can therefore be considered as one-layer stochastic normalizing flow. For a recent application of VAEs as priors in inverse problems in imaging we refer to [21]. Finally, the authors of [40] proposed to reduce the dimension in a first step by a non-variational autoencoder and the optimization of a normalizing flow in the reduced dimensions in a second step.

## 2. Preliminaries

Let  $(\Omega, \mathcal{A}, \mathbb{P})$  be a probability space. By a probability measure on  $\mathbb{R}^d$  we always mean a probability measure defined on the Borel  $\sigma$ -algebra  $\mathcal{B}(\mathbb{R}^d)$ . Let  $\mathcal{P}(\mathbb{R}^d)$  denote the set of probability measures on  $\mathbb{R}^d$ . Given a random variable  $X : \Omega \rightarrow \mathbb{R}^d$ , we use the push-forward notation

$$P_X = X_{\#}\mathbb{P} := \mathbb{P} \circ X^{-1}$$

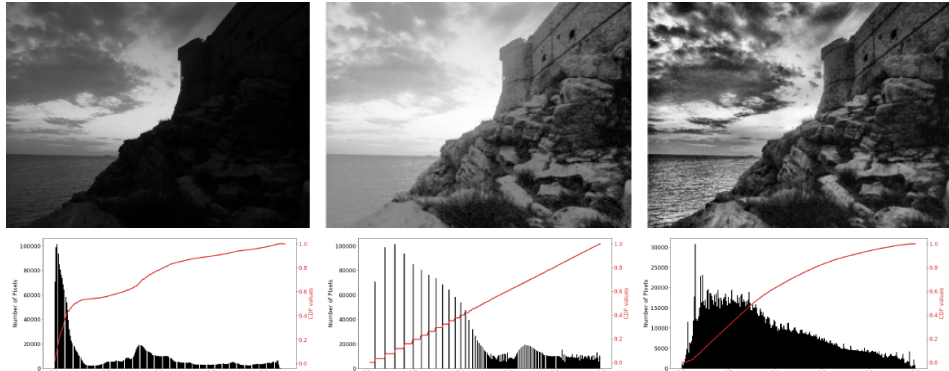
for the corresponding measure on  $\mathbb{R}^d$ . A measure  $\mu \in \mathcal{P}(\mathbb{R}^d)$  is *absolutely continuous* with respect to  $\nu$  and we write  $\mu \ll \nu$  if for every  $B \in \mathcal{B}(\mathbb{R}^d)$  with  $\nu(B) = 0$  we have  $\mu(B) = 0$ . If  $\mu, \nu \in \mathcal{P}(\mathbb{R}^d)$  satisfy  $\mu \ll \nu$ , then the *Radon-Nikodym derivative*  $\frac{d\mu}{d\nu} = \rho \in L^1(\mathbb{R}^d, \nu)$  exists and  $\mu = \rho\nu$ . Special probability measures are

- finite discrete measures

$$\mu = \sum_{j=1}^N \mu_j \delta_{x_j}, \quad \mu_j > 0, \quad \sum_{j=1}^N \mu_j = 1, \quad x_j \in \mathbb{R}^d,$$

where  $\delta_x(B) := 1$  if  $x \in B$  and  $\delta_x(B) := 0$  otherwise. If  $\mu_j = \frac{1}{N}$  for all  $j = 1, \dots, N$ , then these measures are also known as *empirical measures* and otherwise as *atomic measures*.

- measures with densities, i.e. they are absolutely continuous with respect to the Lebesgue measure  $\lambda$  and their density is  $\frac{d\mu}{d\lambda}$ .



Histograms of images as empirical densities and cumulative density function.

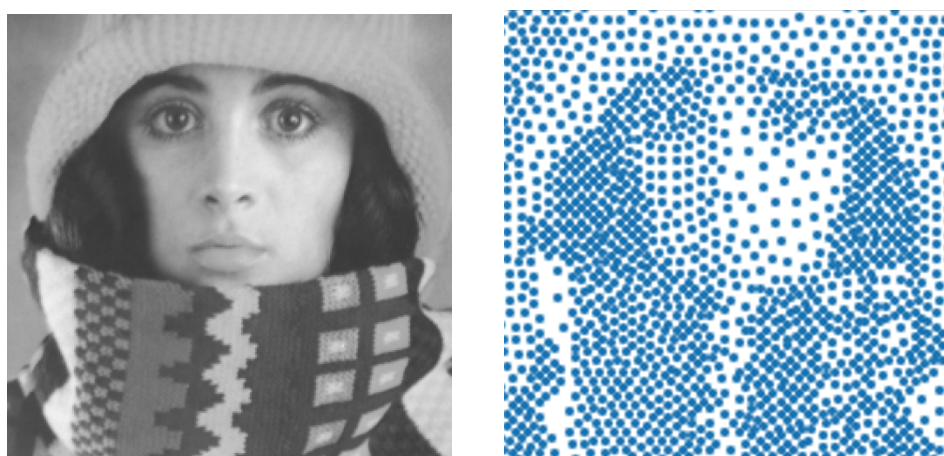
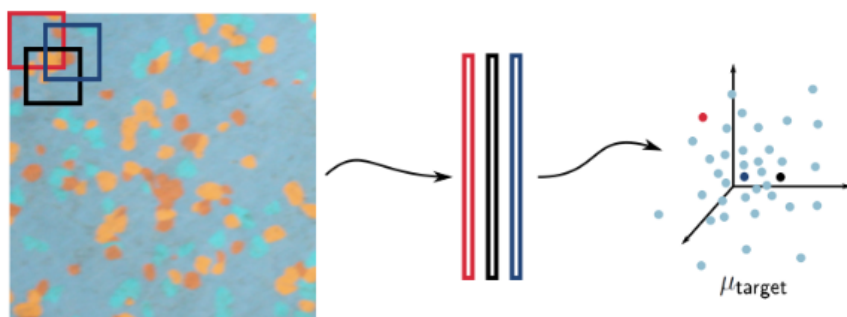


Image as density function on  $\mathbb{R}^2$  and as discrete measure at stippled points.



Images patches of size  $4 \times 4$  rearranged as empirical measure on  $\mathbb{R}^{16}$

Figure 2.3: Different possibilities to assign measures to images as used in [58], [31], [33].

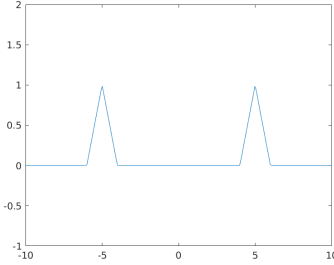


Figure 2.4: Density functions defined below with  $a = 5$ . Define  $M_2(x) := 1 - x$  for  $x \in [0, 1]$  and  $M_2(x) := 1 + x$  for  $x \in (-1, 0)$  and 0 elsewhere and consider the measures  $\mu, \nu$  with densities  $\rho_\mu(x) = M_2(x - a)$  and  $\rho_\nu(x) = M_2(x + a)$ ,  $a > 1$ . Then  $\|\mu - \nu\|_{\text{TV}} = 2$ ,  $\text{KL}(\mu, \nu) = \infty$ , and  $W_1(\mu, \nu) = 2a$ . In particular, the total variation distance does not depend on  $a$ .

Examples, showing why probability measures are interesting in image processing are given in Figure 2.3. It highlights different possibilities to assign probability measures to images.

Probability measures form a special subset of the Banach space of all finite signed Borel measures  $\mathcal{M}(\mathbb{R}^d)$  equipped with the *total variation norm*  $\|\mu\|_{\text{TV}} = |\mu|(\mathbb{R}^d)$ , where

$$|\mu|(B) := \sup \left\{ \sum_{k=1}^{\infty} |\mu(B_k)| : \bigcup_{k=1}^{\infty} B_k = B, B_k \text{ pairwise disjoint} \right\}.$$

It is easier to deal with the total variation norm if we redefine it using the pre-dual space of  $\mathcal{M}(\mathbb{R}^d)$ . Via Riesz' representation theorem the space  $\mathcal{M}(\mathbb{R}^d)$  can be identified with the dual space of the Banach space of bounded, continuous, real-valued functions  $C_b(\mathbb{R}^d)$  equipped with the norm  $\|\varphi\|_{C_b} := \max_{x \in \mathbb{R}^d} |\varphi(x)|$ . Then the total variation norm can be rewritten as

$$\|\mu\|_{\text{TV}} = \sup_{\|\varphi\|_{C_b} \leq 1} \int_{\mathbb{R}^d} \varphi(x) \, d\mu(x), \quad (1)$$

for all  $B \in \mathcal{M}(\mathbb{R}^d)$ . The weak-\* topology on  $\mathcal{M}(\mathbb{R}^d)$  gives rise to the *weak convergence of measures*. More precisely, a sequence  $(\mu_n)_{n \in \mathbb{N}} \subset \mathcal{M}(\mathbb{R}^d)$  converges *weakly* to  $\mu$  and we write  $\mu_n \rightharpoonup \mu$ , if

$$\lim_{n \rightarrow \infty} \int_{\mathbb{R}^d} \varphi \, d\mu_n(x) = \int_{\mathbb{R}^d} \varphi \, d\mu(x) \quad \text{for all } \varphi \in C_b(\mathbb{R}^d).$$

If  $\mathbb{P}_{X_n} \rightharpoonup \mathbb{P}$ , then the corresponding sequence of random variables  $(X_n)_n$  converges in distribution.

The total variation is in general not suited to measure the distance between measures since it doesn't take spatial distances into account and is clumsy to compute. This is illustrated in Figure 2.4. In this tutorial we will apply two other „distance“ functions, namely the Kullback-Leibler divergence and the Wasserstein-1 distance.

For  $\mu, \nu \in \mathcal{P}(\mathbb{R}^d)$  with existing Radon-Nikodym derivative  $\rho = \frac{d\mu}{d\nu}$  of  $\mu$  with respect to  $\nu$ , the *Kullback-Leibler divergence* is defined by

$$\text{KL}(\mu, \nu) := \int_{\mathbb{R}^d} \log \rho \, d\mu(x).$$

In case that the above Radon-Nikodym derivative does not exist, we set  $\text{KL}(\mu, \nu) := +\infty$ . In particular, we have for measures  $\mu, \nu \in \mathcal{P}(\mathbb{R}^d)$  which are absolutely continuous with respect to the Lebesgue measure with densities  $\rho_\mu, \rho_\nu$  that

$$\text{KL}(\mu, \nu) = \int_{\mathbb{R}^d} \log\left(\frac{\rho_\mu}{\rho_\nu}\right) \rho_\mu dx,$$

for discrete probability measures  $\mu = \sum_{j=1}^n \mu_j \delta_{x_j}$  and  $\nu = \sum_{j=1}^n \nu_j \delta_{x_j}$  that

$$\text{KL}(\mu, \nu) = \sum_{j=1}^n \log\left(\frac{\mu_j}{\nu_j}\right) \mu_j.$$

The Kullback-Leibler divergence is a so-called Bregman distance of the Shannon entropy. It has the nice property that  $\text{KL}(\mu, \nu) \geq 0$  for all  $\mu, \nu \in \mathcal{P}(\mathbb{R}^d)$  with equality if and only if  $\mu = \nu$ . On the other hand, it is neither symmetric nor fulfills the triangle inequality. By Pinsker's inequality it holds for all  $\mu, \nu \in \mathcal{P}(\mathbb{R}^d)$  that

$$\|\mu - \nu\|_{\text{TV}}^2 \leq 2\text{KL}(\mu, \nu).$$

For  $p \in [1, \infty)$ , the  $p$ -Wasserstein distance  $W_p$  between measures  $\mu, \nu \in \mathcal{P}(\mathbb{R}^d)$  with finite  $p$ -th moments is defined by

$$W_p(\mu, \nu) := \left( \inf_{\pi \in \Pi(\mu, \nu)} \int_{\mathbb{R}^d \times \mathbb{R}^d} \|x - y\|^p d\pi(x, y) \right)^{\frac{1}{p}},$$

where  $\Pi(\mu, \nu)$  denotes the measures on  $\mathbb{R}^d \times \mathbb{R}^d$  with marginals  $\mu$  and  $\nu$ . It is a metric on the set of measures from  $\mathcal{P}(\mathbb{R}^d)$  with finite  $p$ -th moments, which metrizes the weak topology, i.e.,  $\lim_{n \rightarrow \infty} W_p(\mu_n, \mu) = 0$  if and only if  $\mu_n \rightharpoonup \mu$  and

$$\int_{\mathbb{R}^d} \|x\|^p d\mu_n(x) \rightarrow \int_{\mathbb{R}^d} \|x\|^p d\mu(x)$$

as  $n \rightarrow \infty$ . For  $1 \leq p \leq q < \infty$  it holds  $W_p \leq W_q$ . The distance  $W_1$  is also called *Kantorovich-Rubinstein distance* or *Earth's mover distance*. Switching to the dual problem the Wasserstein-1 distance can be rewritten as

$$W_1(\mu, \nu) = \max_{|\varphi|_{\text{Lip}} \leq 1} \int_{\mathbb{R}^d} \varphi d(\mu - \nu),$$

where the maximum is taken over all Lipschitz continuous functions with Lipschitz constant bounded by 1. This looks similar to the total variation (1), but the space of test functions is smaller for  $W_1$ .

### 3. Markov Kernels

In this section, we introduce the basic notation of Markov kernels and chains, see, e.g., [41].

A *Markov kernel*  $\mathcal{K}: \mathbb{R}^n \times \mathcal{B}(\mathbb{R}^d) \rightarrow [0, 1]$  is a mapping such that

- i)  $\mathcal{K}(\cdot, B)$  is measurable for any  $B \in \mathcal{B}(\mathbb{R}^d)$ , and
- ii)  $\mathcal{K}(x, \cdot)$  is a probability measure for any  $x \in \mathbb{R}^n$ .

For  $\mu \in \mathcal{P}(\mathbb{R}^n)$ , the measure  $\mu \times \mathcal{K}$  on  $\mathbb{R}^n \times \mathbb{R}^d$  is defined by

$$(\mu \times \mathcal{K})(A \times B) := \int_A \mathcal{K}(x, B) d\mu(x). \quad (2)$$

Note that this definition captures all sets in  $\mathcal{B}(\mathbb{R}^n \times \mathbb{R}^d)$  since the measurable rectangles form a  $\cap$ -stable generator of  $\mathcal{B}(\mathbb{R}^n \times \mathbb{R}^d)$ . Then, it holds for all integrable  $f$  that

$$\int_{\mathbb{R}^n \times \mathbb{R}^d} f(x, y) d(\mu \times \mathcal{K})(x, y) = \int_{\mathbb{R}^n} \int_{\mathbb{R}^d} f(x, y) d\mathcal{K}(x, \cdot)(y) d\mu(x).$$

Analogously to (2), we define the product of a measure  $\mu \in \mathcal{P}(\mathbb{R}^{d_0})$  and Markov kernels  $\mathcal{K}_t: \mathbb{R}^{d_{t-1}} \times \mathcal{B}(\mathbb{R}^{d_t}) \rightarrow [0, 1]$  by

$$\begin{aligned} & (\mu \times \mathcal{K}_1 \times \cdots \times \mathcal{K}_T)(A_0 \times \cdots \times A_T) \\ &:= \int_{A_0} \int_{A_1} \cdots \int_{A_{T-1}} \mathcal{K}(x_{T-1}, A_T) d\mathcal{K}(x_{T-2}, \cdot)(x_{T-1}) \cdots d\mathcal{K}(x_0, \cdot)(x_1) d\mu(x_0). \end{aligned}$$

In the following, we use the notion of the *regular conditional distribution* of a random variable  $X$  given a random variable  $Y$  which is defined as the  $P_Y$ -almost surely unique Markov kernel  $P_{Y|X=\cdot}(\cdot)$  with the property

$$P_X \times P_{Y|X=\cdot}(\cdot) = P_{(X, Y)}. \quad (3)$$

We will use the abbreviation  $P_{Y|X} = P_{Y|X=\cdot}(\cdot)$  if the meaning is clear from the context.

A sequence  $(X_0, \dots, X_T)$ ,  $T \in \mathbb{N}$  of  $d_t$ -dimensional random variables  $X_t$ ,  $t = 0, \dots, T$ , is called a *Markov chain*, if there exist Markov kernels

$$\mathcal{K}_t = P_{X_t|X_{t-1}}: \mathbb{R}^{d_{t-1}} \times \mathcal{B}(\mathbb{R}^{d_t}) \rightarrow [0, 1]$$

in the sense (3) such that it holds

$$P_{(X_0, \dots, X_T)} = P_{X_0} \times P_{X_1|X_0} \times \cdots \times P_{X_T|X_{T-1}}. \quad (4)$$

The Markov kernels  $\mathcal{K}_t$  are also called *transition kernels*. If the measure  $\mathcal{K}_t(x, \cdot) = P_{X_t|X_{t-1}=x}$  has a density  $k_t(x, y)$ , and  $P_{X_{t-1}}$  resp.  $P_{X_t}$  have densities  $p_{X_{t-1}}$  resp.  $p_{X_t}$ , then setting  $A := \mathbb{R}^{d_{t-1}}$  in equation (2) results in

$$p_{X_t}(y) = \int_{\mathbb{R}^{d_{t-1}}} k_t(x, y) p_{X_{t-1}}(x) dx.$$

## 4. Normalizing Flows

In this section, we show how normalizing flows can be interpreted as finite Markov chains. A *normalizing flow* is often understood as deterministic, invertible transform, which we call  $\mathcal{T}_\theta: \mathbb{R}^d \rightarrow \mathbb{R}^d$ , see [49]. In this tutorial,  $\mathcal{T}_\theta$  will be an invertible neural network. A brief

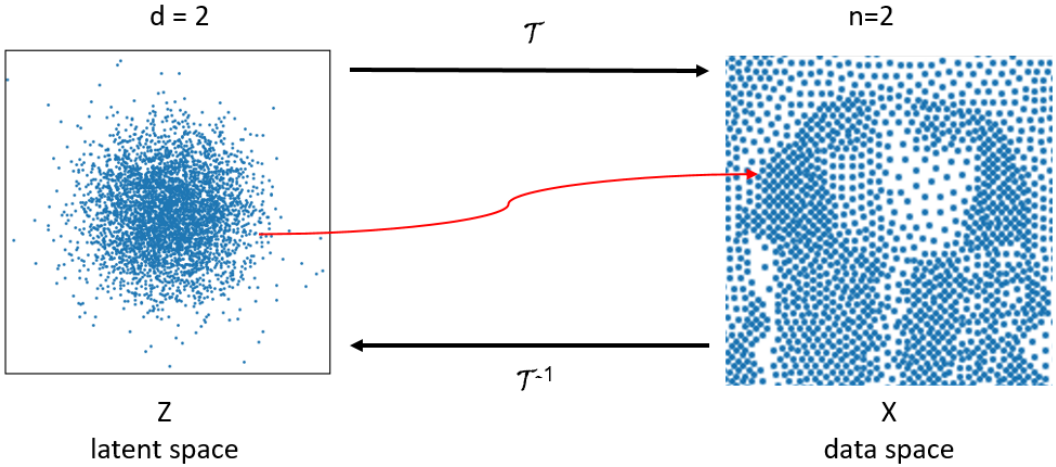


Figure 4.5: Illustration of generative modeling. The invertible NN  $\mathcal{T} : \mathbb{R}^2 \rightarrow \mathbb{R}^2$  maps samples from the latent standard normal distribution to the target distribution.

description of such networks is given in the Appendix A. For better readability, we likewise skip the dependence of  $\mathcal{T}_\theta$  on the parameter  $\theta$  and write just  $\mathcal{T} = \mathcal{T}_\theta$ . Normalizing flows can be used to model the target density  $p_X$  of a distribution  $P_X$  by a simpler latent distribution  $P_Z$  which is usually the standard normal distribution. For an illustration see Figure 4.5. This is done by learning  $\mathcal{T}$  such that it holds

$$P_X \approx \mathcal{T}_\# P_Z, \quad \text{or equivalently} \quad P_Z \approx \mathcal{T}_\#^{-1} P_X.$$

Note that we have by the change of variable formula for the corresponding densities

$$p_{T_\# P_Z}(x) = p_Z(\mathcal{T}^{-1}(x)) |\det \nabla \mathcal{T}^{-1}(x)|.$$

The approximation can be done by minimizing the Kullback-Leibler divergence

$$\begin{aligned} \text{KL}(P_X, \mathcal{T}_\# P_Z) &= \mathbb{E}_{x \sim P_X} \left[ \log \left( \frac{p_X}{p_{T_\# P_Z}} \right) \right] \\ &= \mathbb{E}_{x \sim P_X} [\log p_X] - \mathbb{E}_{x \sim P_X} [\log p_{T_\# P_Z}] \\ &= \mathbb{E}_{x \sim P_X} [\log p_X] - \mathbb{E}_{x \sim P_X} [\log p_Z \circ \mathcal{T}^{-1}] \\ &\quad - \mathbb{E}_{x \sim P_X} [\log |\det(\nabla \mathcal{T}^{-1})|]. \end{aligned}$$

Noting that the first summand is just a constant, this gives the loss function

$$\mathcal{L}_{\text{NF}}(\theta) := -\mathbb{E}_{x \sim P_X} [\log p_Z \circ \mathcal{T}^{-1}] - \mathbb{E}_{x \sim P_X} [\log |\det(\nabla \mathcal{T}^{-1})|]. \quad (5)$$

The network  $\mathcal{T}$  is constructed by concatenating smaller blocks

$$\mathcal{T} = \mathcal{T}_T \circ \dots \circ \mathcal{T}_1$$

which are invertible networks on their own. Then, the blocks  $\mathcal{T}_t: \mathbb{R}^d \rightarrow \mathbb{R}^d$  generate a pair of Markov chains  $((X_0, \dots, X_T), (Y_T, \dots, Y_0))$  by

$$\begin{aligned} X_0 &\sim P_Z, \quad X_t = \mathcal{T}_t(X_{t-1}) \quad \text{and} \\ Y_T &\sim P_X, \quad Y_{t-1} = \mathcal{T}_t^{-1}(Y_t). \end{aligned}$$

Here, for all  $t = 0, \dots, T$ , the dimension  $d_t$  of the random variables  $X_t$  and  $Y_t$  is equal to  $d$ .

**Lemma 4.1.** *The Markov kernel  $\mathcal{K}_t = P_{X_t|X_{t-1}}: \mathbb{R}^d \times \mathcal{B}(\mathbb{R}^d) \rightarrow [0, 1]$  belonging to the above Markov chains are given by the Dirac distributions*

$$\mathcal{K}_t(x, \cdot) = \delta_{\mathcal{T}_t(x)}, \quad \mathcal{R}_t(x, \cdot) = \delta_{\mathcal{T}_t^{-1}(x)}. \quad (6)$$

*Proof.* For any  $A, B \in \mathcal{B}(\mathbb{R}^d)$  it holds

$$\begin{aligned} P_{(X_{t-1}, X_t)}(A \times B) &= \int_{\mathbb{R}^d} 1_{A \times B}(x_{t-1}, x_t) dP_{(X_{t-1}, X_t)}(x_{t-1}, x_t) \\ &= \int_{\mathbb{R}^d} 1_A(x_{t-1}) 1_B(x_t) dP_{(X_{t-1}, X_t)}(x_{t-1}, x_t). \end{aligned}$$

Since  $P_{(X_{t-1}, X_t)}$  is by definition concentrated on the set  $\{(yx_{t-1}, \mathcal{T}_t(x_{t-1})) : x_{t-1} \in \mathbb{R}^d\}$ , this becomes

$$\begin{aligned} P_{(X_{t-1}, X_t)}(A \times B) &= \int_{\mathbb{R}^d \times \mathbb{R}^d} 1_A(x_{t-1}) 1_B(\mathcal{T}_t(x_{t-1})) dP_{(X_{t-1}, X_t)}(x_{t-1}, x_t) \\ &= \int_A 1_B(\mathcal{T}_t(x_{t-1})) dP_{X_{t-1}}(x_{t-1}) \\ &= \int_A \delta_{\mathcal{T}_t(x_{t-1})}(B) dP_{X_{t-1}}. \end{aligned}$$

Consequently, by (2), the transition kernel  $\mathcal{K}_t = P_{X_t|X_{t-1}}$  is given by  $\mathcal{K}_t(x, \cdot) = \delta_{\mathcal{T}_t(x)}$ .  $\square$

Due to their correspondence to the layers  $\mathcal{T}_t$  and  $\mathcal{T}_t^{-1}$  from the normalizing flow  $\mathcal{T}$ , we call the Markov kernels  $\mathcal{K}_t$  *forward layers*, while the Markov kernels  $\mathcal{R}_t$  are called *reverse layers*.

## 5. Stochastic Normalizing Flows

We have already seen that normalizing flows have a limited expressiveness. The idea of stochastic normalizing flows is to replace some of the deterministic layers  $\mathcal{T}_t$  from a normalizing flow by random transforms. From the Markov chains viewpoint, we replace the kernels  $\mathcal{K}_t$  and  $\mathcal{R}_t$  with the Dirac measure by more general Markov kernels. In Figure 5.6 the interaction of stochastic steps in conjunction with deterministic ones is illustrated. In particular, the stochastic steps effectively remove samples from low density regions.

Formally, a *stochastic normalizing flow* (SNF) is a pair  $((X_0, \dots, X_T), (Y_T, \dots, Y_0))$  of Markov chains of  $d_t$ -dimensional random variables  $X_t$  and  $Y_t$ ,  $t = 0, \dots, T$ , with the following properties:

P1)  $P_{X_t}, P_{Y_t}$  have the densities  $p_{X_t}, p_{Y_t}: \mathbb{R}^{d_t} \rightarrow \mathbb{R}_{>0}$  for any  $t = 0, \dots, T$ .

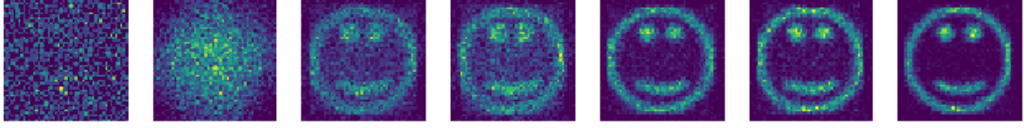


Figure 5.6: The path on which the stochastic normalizing flow moves from the latent density (left most picture) to the target density (right most picture). We alternate invertible neural network layers with MCMC layers, starting with the first one.

P2) There exist Markov kernels  $\mathcal{K}_t = P_{X_t|X_{t-1}}$  and  $\mathcal{R}_t = P_{Y_{t-1}|Y_t}$ ,  $t = 1, \dots, T$  such that

$$\begin{aligned} P_{(X_0, \dots, X_T)} &= P_{X_0} \times P_{X_1|X_0} \times \dots \times P_{X_T|X_{T-1}}, \\ P_{(Y_T, \dots, Y_0)} &= P_{Y_T} \times P_{Y_{T-1}|Y_T} \times \dots \times P_{Y_0|Y_1}. \end{aligned}$$

P3) For  $P_{X_t}$ -almost every  $x \in \mathbb{R}^{d_t}$ , the measures  $P_{Y_{t-1}|Y_t=x}$  and  $P_{X_{t-1}|X_t=x}$  are absolutely continuous with respect to each other.

We say that the Markov chain  $(Y_T, \dots, Y_0)$  is a *reverse Markov chain* of  $(X_0, \dots, X_T)$ , see Lemma B.1 in the appendix. In applications, Markov chains usually start with a latent random variable

$$X_0 = Z$$

on  $\mathbb{R}^{d_0}$ , which is easy to sample from and we intend to learn the Markov chain such that  $X_T$  approximates a target random variable  $X$  on  $\mathbb{R}^{d_T}$ , while the reversed Markov chain is initialized with a random variable

$$Y_T = X$$

from a data space and  $Y_0$  should approximate the latent variable  $Z$ . As outlined in the previous paragraph, each deterministic normalizing flow is a special case of a SNF.

### 5.1. Training SNFs

We aim to find parameters of a SNF such that  $P_{X_T} \approx P_X$ . Recall, that for deterministic normalizing flows, it holds  $P_{X_T} = \mathcal{T}_\# P_Z$ , such that the loss function  $\mathcal{L}_{\text{NF}}$  reads as  $\mathcal{L}_{\text{NF}} = \text{KL}(P_X, P_{X_T})$ . Unfortunately, the stochastic layers make it impossible to evaluate and minimize  $\text{KL}(P_X, P_{X_T})$ . Instead, we minimize the KL divergence of the joint distributions

$$\mathcal{L}_{\text{SNF}} := \text{KL}(P_{(Y_0, \dots, Y_T)}, P_{(X_0, \dots, X_T)}),$$

which is an upper bound of  $\text{KL}(P_{Y_T}, P_{X_T}) = \text{KL}(P_X, P_{X_T})$ , see Lemma B.2 in the appendix. The following theorem was proved in [24], Theorem 5.

**Theorem 5.1.** *The loss function  $\mathcal{L}_{SNF}$  can be rewritten as*

$$\begin{aligned}
\mathcal{L}_{SNF}(\theta) &= \text{KL}(P_{(Y_0, \dots, Y_T)}, P_{(X_0, \dots, X_T)}) \\
&= \mathbb{E}_{(x_0, \dots, x_T) \sim P_{(Y_0, \dots, Y_T)}} \left[ \log \left( \frac{p_X(x_T)}{p_{X_T}(x_T)} \prod_{t=1}^T f_t(x_{t-1}, x_t) \right) \right] \\
&= \mathbb{E}_{(x_0, \dots, x_T) \sim P_{(Y_0, \dots, Y_T)}} \left[ \log \left( \frac{p_X(x_T)}{p_Z(x_0)} \prod_{t=1}^T \frac{f_t(x_{t-1}, x_t) p_{X_{t-1}}(x_{t-1})}{p_{X_t}(x_t)} \right) \right],
\end{aligned} \tag{7}$$

where  $f_t(\cdot, x_t)$  is given by the Radon-Nikodym derivative  $\frac{dP_{Y_{t-1}|Y_t=x_t}}{dP_{X_{t-1}|X_t=x_t}}$ .

For the deterministic NF layers and the stochastic layers discussed in the next section the quotients in the loss function (7) are specified in Theorem 6.4. In particular, Theorem 6.4 yields that we have for any deterministic normalizing flow that  $\mathcal{L}_{NF} = \mathcal{L}_{SNF}$ .

## 6. Stochastic Layers

In this section, we consider different stochastic layers, namely

- Langevin layer,
- Metropolis-Hastings (MH) layer,
- Metropolis-adjusted Langevin (MALA) layer,
- VAE layer,
- diffusion normalizing flow layer.

The first three were used in [24, 64]. Note that further layers were introduced in [45]. In the following, let  $\mathcal{N}(\mu, \Sigma)$  denote the normal distribution with density

$$\mathcal{N}(x; m, \Sigma) := (2\pi)^{-\frac{d}{2}} |\Sigma|^{-\frac{1}{2}} \exp \left( -\frac{1}{2} (x - m)^T \Sigma^{-1} (x - m) \right).$$

### 6.1. Langevin Layer

As for the deterministic layers we choose

$$d_{t-1} = d_t = d.$$

The basic idea is to push the distribution of  $X_{t-1}$  into the direction of some proposal density  $p_t: \mathbb{R}^d \rightarrow \mathbb{R}_{>0}$ , which is usually chosen as some interpolation between  $p_X$  and  $p_Z$ . For a detailed description of this interpolation, we refer to [24]. As reverse layer, we use the same Markov kernel as the forward layer, i.e.,

$$\mathcal{R}_t = \mathcal{K}_t.$$

In the Langevin layer, we model the transition from  $X_{t-1}$  to  $X_t$  by one step of an explicit Euler discretization of the overdamped Langevin dynamics, see [62]. Let  $\xi_t \sim \mathcal{N}(0, I)$  such that  $\sigma(\xi_t)$  and  $\sigma(\cup_{s \leq t-1} \sigma(X_s))$  are independent. Again we assume that we are given a proposal density  $p_t: \mathbb{R}^d \rightarrow \mathbb{R}_{>0}$  which has to be specified. We denote by

$$u_t(x) := -\log(p_t(x))$$

the negative log-likelihood of  $p_t$  and set

$$X_t := X_{t-1} - a_1 \nabla u_t(X_{t-1}) + a_2 \xi_t,$$

where  $a_1, a_2 > 0$  are some predefined constants.

**Lemma 6.1.** *The Markov kernel  $\mathcal{K}_t = P_{X_t|X_{t-1}}: \mathbb{R}^d \times \mathcal{B}(\mathbb{R}^d) \rightarrow [0, 1]$  belonging to the Langevin transition is*

$$\mathcal{K}_t(x, \cdot) := \mathcal{N}(x - a_1 \nabla u_t(x), a_2^2 I). \quad (8)$$

*Proof.* To determine the corresponding kernel, we use the the independence of  $\xi_t$  of  $X_t$  and  $X_{t-1}$  to obtain that  $X_t$  and  $X_{t-1}$  have the common density

$$\begin{aligned} P_{(X_{t-1}, X_t)}(x_{t-1}, x_t) &= p_{X_{t-1}, \xi_t}(x_{t-1}, \frac{1}{a_2}(x_t - x_{t-1} + a_1 \nabla u_t(x_{t-1}))) \\ &= p_{X_{t-1}}(x_{t-1}) p_{\xi_t}(\frac{1}{a_2}(x_t - x_{t-1} + a_1 \nabla u_t(x_{t-1}))) \\ &= p_{X_{t-1}}(x_{t-1}) \mathcal{N}(x_t; x_{t-1} - a_1 \nabla u_t(x_{t-1}), a_2^2 I). \end{aligned}$$

Then, for  $A, B \in \mathcal{B}(\mathbb{R}^d)$ , it holds

$$\begin{aligned} P_{(X_{t-1}, X_t)}(A \times B) &= \int_{A \times B} p_{X_{t-1}}(x_{t-1}) \mathcal{N}(x_t; x_{t-1} - a_1 \nabla u_t(x_{t-1}), a_2^2 I) d(x_{t-1}, x_t) \\ &= \int_A \int_B \mathcal{N}(x_t; x_{t-1} - a_1 \nabla u_t(x_{t-1}), a_2^2 I) dx_t p_{X_{t-1}}(x_{t-1}) dx_{t-1} \\ &= \int_A \mathcal{K}_t(x_{t-1}, B) p_{X_t}(x_t) dP_{X_{t-1}}(x_{t-1}), \end{aligned}$$

where

$$\mathcal{K}_t(x, \cdot) := \mathcal{N}(x - a_1 \nabla u_t(x), a_2^2 I).$$

By (2) and (3) this is the Langevin transition kernel  $P_{X_t|X_{t-1}}$ .  $\square$

## 6.2. Metropolis-Hastings Layer

Again we choose  $d_{t-1} = d_t = d$  and

$$\mathcal{R}_t = \mathcal{K}_t$$

and push the distribution of  $X_{t-1}$  into the direction of some proposal density  $p_t: \mathbb{R}^d \rightarrow \mathbb{R}_{>0}$ .

The Metropolis-Hastings algorithm outlined in Alg. 1 is a frequently used Markov Chain Monte Carlo type algorithm to sample from a proposal distribution  $P$  with known proposal

---

**Algorithm 1** Metropolis-Hastings Algorithm

---

**Input:**  $x_0 \in \mathbb{R}^d$ , proposal density  $p_t: \mathbb{R}^d \rightarrow \mathbb{R}_{>0}$

**For**  $k = 0, 1, \dots$  **do**

Draw  $x'$  from  $\mathcal{N}(x_k, \sigma^2 I)$  and  $u$  uniformly in  $[0, 1]$ .

Compute the acceptance ratio

$$\alpha(x_k, x') := \min \left\{ 1, \frac{p(x')}{p(x_k)} \right\}.$$

Set

$$x_{k+1} := \begin{cases} x' & \text{if } u < \alpha(x_k, x'), \\ x_k & \text{otherwise.} \end{cases}$$

**Output:**  $\{x_k\}_k$

---

density  $p$ , see, e.g., [51]. Under mild assumptions, the corresponding Markov chain  $(X_k)_{k \in \mathbb{N}}$  admits the unique stationary distribution  $P$  and  $P_{X_k} \rightarrow P$  as  $k \rightarrow \infty$  in the total variation norm, see, e.g. [60].

In the MH layer, the transition from  $X_{t-1}$  to  $X_t$  is one step of a Metropolis-Hastings algorithm. More precisely, let  $\xi_t \sim \mathcal{N}(0, \sigma^2 I)$  and  $U \sim \mathcal{U}_{[0,1]}$  be random variables such that  $(\sigma(\xi_t), \sigma(U), \sigma(\cup_{s \leq t-1} \sigma(X_s)))$  are independent. Here  $\sigma(X)$  denotes the smallest  $\sigma$ -algebra generated by the random variable  $X$ . Then, we set

$$X_t := X_{t-1} + 1_{[U,1]}(\alpha_t(X_{t-1}, X_{t-1} + \xi_t)) \xi_t$$

where

$$\alpha_t(x, y) := \min \left\{ 1, \frac{p_t(y)}{p_t(x)} \right\}$$

with a proposal density  $p_t$  which has to be specified.

**Lemma 6.2.** *The Markov kernel  $\mathcal{K}_t = P_{X_t|X_{t-1}}: \mathbb{R}^d \times \mathcal{B}(\mathbb{R}^d) \rightarrow [0, 1]$  belonging to the Metropolis-Hastings transition is*

$$\begin{aligned} \mathcal{K}_t(x, A) &:= \int_A \mathcal{N}(y; x, \sigma^2 I) \alpha_t(x, y) dy \\ &+ \delta_x(A) \int_{\mathbb{R}^d} \mathcal{N}(y; x, \sigma^2 I) (1 - \alpha_t(x, y)) dy. \end{aligned} \tag{9}$$

The proof is a special case of Lemma B.3 in the appendix.

### 6.3. Metropolis-adjusted Langevin Layer

Another kind of MH layer comes from the Metropolis-adjusted Langevin algorithm (MALA), see [20, 52]. Again we choose  $d_{t-1} = d_t = d$  and

$$\mathcal{R}_t = \mathcal{K}_t$$

and push the distribution of  $X_{t-1}$  into the direction of some proposal density  $p_t: \mathbb{R}^d \rightarrow \mathbb{R}_{>0}$ . Let  $\xi_t \sim \mathcal{N}(0, I)$ ,  $a_1, a_2 > 0$  and  $u_t := -\log p_t$  as in the Langevin layer. Further, we choose

$$Q_t(x, \cdot) := \mathcal{N}(x - a_1 \nabla u_t(x), a_2^2 I), \quad q(\cdot|x) := \mathcal{N}(\cdot|x - a_1 \nabla u_t(x), a_2^2 I).$$

Then the Metropolis-adjusted Langevin algorithm is detailed in Alg. 2.

---

**Algorithm 2** Metropolis adjusted Langevin Algorithm

---

**Input:**  $x_0 \in \mathbb{R}^d$ , proposal density  $p_t: \mathbb{R}^d \rightarrow \mathbb{R}_{>0}$ ,  $a_1, a_2 > 0$

**For**  $k = 0, 1, \dots$  **do**

Draw  $x'$  from  $\mathcal{N}(x_k - a_1 \nabla u_t(x_k), a_2^2 I)$  and  $u$  uniformly in  $[0, 1]$ .

Compute the acceptance ratio

$$\alpha(x_k, x') := \min \left\{ 1, \frac{p(x')q(x_k|x')}{p(x_k)q(x'|x_k)} \right\}.$$

Set

$$x_{k+1} := \begin{cases} x' & \text{if } u < \alpha(x_k, x'), \\ x_k & \text{otherwise.} \end{cases}$$

**Output:**  $\{x_k\}_k$

---

In the MALA layer, the transition from  $X_{t-1}$  to  $X_t$  is one step of a MALA algorithm. More precisely, we set

$$X_t := X_{t-1} + 1_{[U,1]} (\alpha_t(X_{t-1}, X_{t-1} - a_1 \nabla u_t(X_{t-1}) + a_2 \xi_t)) (a_2 \xi_t - a_1 \nabla u_t(X_{t-1})),$$

where  $\alpha_t$  is defined as in the MALA algorithm. The corresponding Markov kernel is determined by the following lemma.

**Lemma 6.3.** *The Markov kernel  $\mathcal{K}_t = P_{X_t|X_{t-1}}: \mathbb{R}^d \times \mathcal{B}(\mathbb{R}^d) \rightarrow [0, 1]$  belonging to the MALA transition is*

$$\begin{aligned} \mathcal{K}_t(x, A) &:= \int_A q_t(y|x) \alpha_t(x, y) dy \\ &\quad + \delta_x(A) \int_{\mathbb{R}^d} q_t(y|x) (1 - \alpha_t(x, y)) dy. \end{aligned} \tag{10}$$

The proof is a special case of Lemma B.3 in the appendix.

#### 6.4. VAE Layer

In this section, we introduce variational autoencoders (VAEs) as another kind of stochastic layers of a SNF. First, we briefly revisit the definition of autoencoders and VAEs. Afterwards, we show that a VAE can be viewed as a one-layer SNF.

**Autoencoders.** Autoencoders are a dimensionality reduction technique inspired by the principal component analysis. For an overview, see, e.g. [22]. For  $d > n$ , an autoencoder is a pair  $(E, D)$  of neural networks, consisting of an encoder  $E = E_\phi: \mathbb{R}^d \rightarrow \mathbb{R}^n$  and a decoder  $D = D_\theta: \mathbb{R}^n \rightarrow \mathbb{R}^d$ , where  $\theta$  and  $\phi$  are the neural networks parameters. The network  $E$  aims to encode samples  $x$  from a  $d$ -dimensional distribution  $P_X$  in the lower-dimensional space  $\mathbb{R}^n$  such that the decoder  $D$  is able to reconstruct them. Consequently, it is a necessary assumption that the distribution  $P_X$  is approximately concentrated on a  $n$ -dimensional manifold. A possible loss function to train  $E_\phi$  and  $D_\theta$  is given by

$$\mathcal{L}_{\text{AE}}(\phi, \theta) := \mathbb{E}_{x \sim P_X} [\|x - D_\theta(E_\phi(x))\|^2].$$

Using this construction, autoencoders have shown to be very powerful for reduce the dimensionality of very complex datasets.

**Variational Autoencoders via Markov Kernels.** Variational autoencoders (VAEs) originally introduced in [38], aim to use the power of autoencoders to approximate a probability distribution  $P_X$  with density  $p_X$  using a simpler distribution  $P_Z$  with density  $p_Z$  which is usually the standard normal distribution. Here, the idea is to learn random transforms that push the distribution  $P_X$  onto  $P_Z$  and vice versa. Formally, these transforms are defined by the Markov kernels

$$\mathcal{K}(z, \cdot) := \mathcal{N}(\mu_\theta(z), \Sigma_\theta(z)) \quad \text{and} \quad \mathcal{R}(x, \cdot) := \mathcal{N}(\mu_\phi(x), \Sigma_\phi(x)), \quad (11)$$

where

$$D(z) = D_\theta(z) := (\mu_\theta(z), \Sigma_\theta(z))$$

is a neural network with parameters  $\theta$ , which determines the parameters of the normal distribution within the definition of  $\mathcal{K}$ . Similarly,

$$E(x) = E_\phi(x) := (\mu_\phi(x), \Sigma_\phi(x))$$

determines the parameters within the definition of  $\mathcal{R}$ . In analogy to the autoencoders in the previous paragraph,  $D$  and  $E$  are called stochastic decoder and encoder. By definition,  $\mathcal{K}(z, \cdot)$  has the density  $p_\theta(x|z) = \mathcal{N}(x; \mu_\theta(z), \Sigma_\theta(z))$  and  $\mathcal{R}(x, \cdot)$  has the density  $q_\phi(z|x) = \mathcal{N}(z; \mu_\phi(x), \Sigma_\phi(x))$ .

Now, we aim to learn the parameters  $\theta$  such that it holds approximately

$$p_X(x) \approx \int_{\mathbb{R}^n} p_\theta(x|z) p_Z(z) dz$$

or equivalently

$$P_X(A) \approx \int_{\mathbb{R}^n} \mathcal{K}(z, A) dP_Z(z).$$

Assuming that the above equation holds true exactly, we can generate samples from  $P_X$  by first sampling  $z$  from  $P_Z$  and then sampling  $x$  from  $\mathcal{K}(z, \cdot)$ .

The first idea would be to use the maximum likelihood estimator as loss function, i.e., maximize

$$\mathbb{E}_{x \sim P_X} [\log(p_\theta(x))], \quad p_\theta(x) = \int_{\mathbb{R}^n} p_\theta(x|z) p_Z(z) dz.$$

Unfortunately, computing the integral directly is intractable. Thus, using Bayes' formula

$$p_\theta(z|x) = \frac{p_\theta(x|z)p_Z(z)}{p_\theta(x)},$$

we artificially incorporate the stochastic encoder by the computation

$$\begin{aligned} \log(p_\theta(x)) &= \mathbb{E}_{z \sim q_\phi(\cdot|x)} \left[ \log \left( \frac{p_\theta(x)p_\theta(z|x)}{p_\theta(z|x)} \right) \right] \\ &= \mathbb{E}_{z \sim q_\phi(\cdot|x)} \left[ \log \left( \frac{p_\theta(x)p_\theta(z|x)}{q_\phi(z|x)} \right) \right] + \mathbb{E}_{z \sim q_\phi(\cdot|x)} \left[ \log \left( \frac{q_\phi(z|x)}{p_\theta(z|x)} \right) \right] \\ &= \mathbb{E}_{z \sim q_\phi(\cdot|x)} \left[ \log \left( \frac{p_\theta(x|z)p_Z(z)}{q_\phi(z|x)} \right) \right] + \text{KL}(q_\phi(\cdot|x), p_\theta(\cdot|x)) \\ &\geq \mathbb{E}_{z \sim q_\phi(\cdot|x)} \left[ \log \left( \frac{p_\theta(x|z)p_Z(z)}{q_\phi(z|x)} \right) \right] \end{aligned}$$

Then the loss function

$$\mathcal{L}_{\theta, \phi}(x) := \mathbb{E}_{z \sim q_\phi(\cdot|x)} \left[ \log(p_\theta(x|z)p_Z(z)) - \log(q_\phi(z|x)) \right] \quad (12)$$

is a lower bound on the so-called evidence  $\log(p_\theta(x))$ . Therefore it is called the *evidence lower bound (ELBO)*. Now the parameters  $\theta$  and  $\phi$  of the VAE  $(E_\phi, D_\theta)$  can be trained by maximizing the expected ELBO, i.e., by minimizing the loss function

$$\mathcal{L}_{\text{VAE}}(\theta, \phi) = -\mathbb{E}_{x \sim P_X} [\mathcal{L}_{\theta, \phi}(x)]. \quad (13)$$

**VAEs as One Layer SNFs.** In the following, we show that a VAE is a special case of one layer SNF. Let  $((X_0, X_1), (Y_1, Y_0))$  be a one-layer SNF, where the layers  $\mathcal{K}_1 = \mathcal{K} = P_{X_1|Z}$  and  $\mathcal{R}_1 = \mathcal{R} = P_{Y_0|X}$  are defined as in (11) with densities  $p_\theta(\cdot|z)$  and  $q_\phi(\cdot|x)$ , respectively. Note that in contrast to the stochastic layers from Section 5 the dimensions  $d_0$  and  $d_1$  are no longer equal. Now, with  $X_0 = Z$ , the loss function (7) of the SNF reads as

$$\mathcal{L}_{\text{SNF}}(\theta, \phi) = \mathbb{E}_{(z, x) \sim P_{(Y_0, Y_1)}} \left[ -\log \left( \frac{p_{X_1}(x)}{p_X(x)f_1(z, x)} \right) \right], \quad (14)$$

where  $f_1(\cdot, x)$  is given by the Radon-Nikodym derivative  $\frac{dP_{Y_0|Y_1=x}}{dP_{X_0|X_1=x}}$ . Now we can use that by the definition of  $\mathcal{K}$  and  $\mathcal{R}$  the random variables  $(Y_0, Y_1)$  as well as the random variables  $(X_0, X_1)$  have a joint density. Hence  $f_1$  can be expressed by the corresponding densities  $p_{X_0|X_1=x}$  of  $p_{Y_0|Y_1=x}$ . Together with Bayes' formula we obtain

$$f_1(z, x) = \frac{p_{Y_0|Y_1=x}(z)}{p_{X_0|X_1=x}(z)} = \frac{q_\phi(z|x)}{p_{X_1|X_0=z}(x)} \frac{p_{X_1}(x)}{p_{X_0}(z)} = \frac{q_\phi(z|x)}{p_\theta(x|z)} \frac{p_{X_1}(x)}{p_Z(z)}. \quad (15)$$

Inserting this into (14), we get

$$\mathcal{L}_{\text{SNF}}(\theta, \phi) = \mathbb{E}_{(z, x) \sim P_{(Y_0, Y_1)}} \left[ -\log \left( \frac{p_\theta(x|z)p_Z(z)}{q_\phi(z|x)p_X(x)} \right) \right]$$

and using (3) further

$$\begin{aligned}
\mathcal{L}_{\text{SNF}}(\theta, \phi) &= \mathbb{E}_{x \sim P_X} \left[ \mathbb{E}_{z \sim \mathcal{R}(x, \cdot)} \left[ -\log \left( \frac{p_\theta(x|z)p_Z(z)}{q_\phi(z|x)p_X(x)} \right) \right] \right] \\
&= \mathbb{E}_{x \sim P_X} \left[ \mathbb{E}_{z \sim q_\phi(\cdot|x)} \left[ -\log \left( \frac{p_\theta(x|z)p_Z(z)}{q_\phi(z|x)} \right) \right] \right] + \mathbb{E}_{x \sim P_X} [\log(p_X(x))] \\
&= -\mathbb{E}_{x \sim P_X} [\mathcal{L}_{\theta, \phi}(x)] + \mathbb{E}_{x \sim P_X} [\log(p_X(x))],
\end{aligned}$$

where  $\mathcal{L}_{\theta, \phi}$  denotes the ELBO as defined in (12) and  $\mathbb{E}_{x \sim P_X} [\log(p_X(x))]$  is a constant independent of  $\theta$  and  $\phi$ . Consequently, minimizing  $\mathcal{L}_{\text{SNF}}(\theta, \phi)$  is equivalent to minimize the negative expected ELBO, which is exactly the loss  $\mathcal{L}_{\text{VAE}}(\theta, \phi)$  for VAEs from (13).

The above result could alternatively be derived via the relation of the ELBO to the KL divergence between the probability measures defined by the densities  $(x, z) \mapsto p_\theta(x|z)p_Z(z)$  and  $(x, z) \mapsto q_\phi(z|x)p_X(x)$ , see [39, Section 2.7].

## 6.5. Diffusion Normalizing Flow Layer

Recently, the authors of [57] proposed to learn the drift  $f_t: \mathbb{R}^d \rightarrow \mathbb{R}^d$ ,  $t \in [0, S]$  and diffusion coefficient  $g_t \in \mathbb{R}$  of a stochastic differential equation

$$dX_t = f_t(X_t)dt + g_t dB_t \quad (16)$$

with respect to the Brownian motion  $B_t$ , such that it holds approximately  $X_S \sim P_X$  for some  $S > 0$  and some data distribution  $P_X$ . The explicit Euler discretization of (16) with step size  $\epsilon > 0$  reads as

$$X_t = X_{t-1} + \epsilon f_{t-1}(X_{t-1}) + \sqrt{\epsilon} g_{t-1} \xi_{t-1}, \quad t = 1, \dots, T,$$

where  $\xi_{t-1} \sim \mathcal{N}(0, I)$  is independent of  $X_0, \dots, X_{t-1}$ . With a similar computation as for the Langevin layers, this corresponds to the Markov kernel

$$\mathcal{K}_t(x, \cdot) = P_{X_t|X_{t-1}=x} = \mathcal{N}(x + \epsilon f_{t-1}(x), \epsilon g_{t-1}^2). \quad (17)$$

Song et. al. parametrized the functions  $f_t: \mathbb{R}^d \rightarrow \mathbb{R}^d$  by some a-priori learned score network, see [35, 56], and achieved competitive performance in image generation. Motivated by the time-reversal process, [1, 27, 17] of the SDE (16), Zhang and Chen [65] introduced the backward layer

$$\mathcal{R}_t(x, \cdot) = P_{Y_{t-1}|Y_t=x} = \mathcal{N}(x + \epsilon(f_t(x) - g_t^2 s_t(x)), \epsilon g_t^2)$$

and learn the parameters of the neural networks  $f_t: \mathbb{R}^d \rightarrow \mathbb{R}^d$  and  $s_t: \mathbb{R}^d \rightarrow \mathbb{R}^d$  using the loss function  $\mathcal{L}_{\text{SNF}}$  from (7) to achieve state-of-the-art results. Even though Zhang and Chen call their model diffusion flow, it is indeed a special case of a SNF using the forward and backward layers  $\mathcal{K}_t$  and  $\mathcal{R}_t$ .

On the other hand, not every SNF can be represented as a discretized SDE. For example, the forward layer (9) from the MH layer has not the form (17).

## 6.6. Training of Stochastic Layers

For the training of SNFs with the loss function  $\mathcal{L}_{\text{SNF}}$  from (7), we have to compute the quotients  $\frac{f_t(x_{t-1}, x_t) p_{X_{t-1}}(x_{t-1})}{p_{X_t}(x_t)}$  for every layer. The next theorem specifies, how this can be done for deterministic NF layers and the stochastic layers introduced in this section.

**Theorem 6.4.** *Let  $(X_0, \dots, X_T)$  be a Markov chain with a reverse  $(Y_T, \dots, Y_0)$  and  $(x_0, \dots, x_T) \in \text{supp}(P_{(X_0, \dots, X_T)}) = \text{supp}(P_{(Y_0, \dots, Y_T)})$ . Let  $f_t(\cdot, x_t)$  be the Radon-Nikodym derivative  $\frac{dP_{Y_{t-1}|Y_t=x_t}}{dP_{X_{t-1}|X_t=x_t}}$ . Then the following holds true:*

i) *For the deterministic layer determined by (6):*

$$\frac{p_{X_{t-1}}(x_{t-1})}{p_{X_t}(x_t)} = \frac{1}{|\nabla \mathcal{T}_t^{-1}(x_t)|} \quad \text{and} \quad f_t(x_{t-1}, x_t) = 1.$$

ii) *For the Langevin layer in (8):*

$$\frac{f_t(x_{t-1}, x_t) p_{X_{t-1}}(x_{t-1})}{p_{X_t}(x_t)} = \exp\left(\frac{1}{2}(\|\eta_t\|^2 - \|\tilde{\eta}_t\|^2)\right),$$

where

$$\eta_t := \frac{1}{a_2}(x_{t-1} - x_t - a_1 \nabla u_t(x_{t-1})), \quad \tilde{\eta}_t := \frac{1}{a_2}(x_{t-1} - x_t + a_1 \nabla u_t(x_t)).$$

iii) *For the MH layer determined by (9):*

$$\frac{f_t(x_{t-1}, x_t) p_{X_{t-1}}(x_{t-1})}{p_{X_t}(x_t)} = \frac{p_t(x_{t-1})}{p_t(x_t)}.$$

iv) *For the MALA layer given by (10):*

$$\frac{f_t(x_{t-1}, x_t) p_{X_{t-1}}(x_{t-1})}{p_{X_t}(x_t)} = \frac{p_t(x_{t-1})}{p_t(x_t)}.$$

v) *For the VAE layer in (11):*

$$\frac{f_t(x_{t-1}, x_t) p_{X_{t-1}}(x_{t-1})}{p_{X_t}(x_t)} = \frac{q_\phi(x_{t-1}|x_t)}{p_\theta(x_t|x_{t-1})}$$

vi) *For the diffusion normalizing flow layer in (17):*

$$\frac{f_t(x_{t-1}, x_t) p_{X_{t-1}}(x_{t-1})}{p_{X_t}(x_t)} = \exp\left(\frac{1}{2}(\|\eta_t\|^2 - \|\tilde{\eta}_t\|^2)\right),$$

where

$$\begin{aligned} \eta_t &:= \frac{1}{\sqrt{\epsilon} g_{t-1}}(x_{t-1} - x_t + \epsilon f_{t-1}(x_{t-1})), \\ \tilde{\eta}_t &:= \frac{1}{\sqrt{\epsilon} g_t}(x_{t-1} - x_t - \epsilon(f_t(x_t) - g_t^2 s_t(x_t))). \end{aligned}$$

The assertions i)-iv) were proved in [24], while v) follows from equation (15) and the derivation of vi) is analogously to ii).

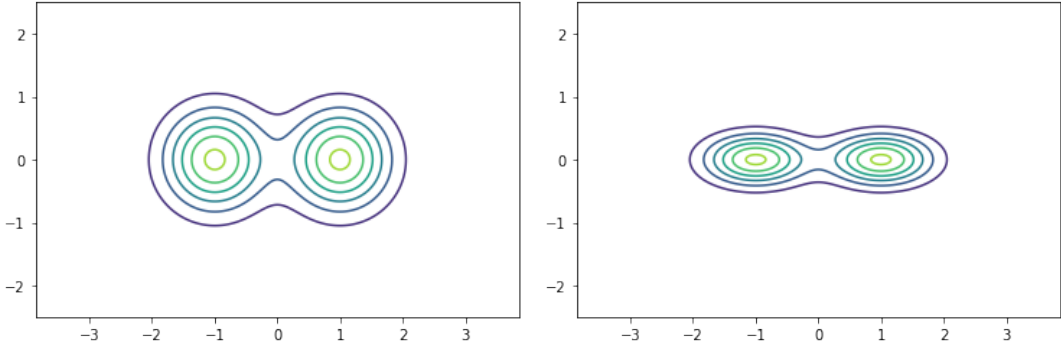


Figure 7.7: Illustration of the prior density  $p_X$  (left) and the posterior density  $p_{X|Y=y}$  for  $y = 0$  (right) within the inverse problem (18) with  $F(x_1, x_2) = x_2$  and  $\eta \sim \mathcal{N}(0, 0.1^2)$ .

## 7. Conditional Generative Modeling

So far we have considered the task of sampling from  $P_X$  using a simpler distribution  $P_Z$ . For inverse problems, we have to adjust our setting. Let  $X: \Omega \rightarrow \mathbb{R}^d$  be a random variable and let  $Y: \Omega \rightarrow \mathbb{R}^{\tilde{d}}$  be defined by

$$Y = F(X) + \eta, \quad (18)$$

for some (ill-posed), not necessary linear operator  $F: \mathbb{R}^d \rightarrow \mathbb{R}^{\tilde{d}}$  and a random variable  $\eta: \Omega \rightarrow \mathbb{R}^{\tilde{d}}$ . In the following, we aim to find the posterior distribution  $P_{X|Y=y}$  for some measurement  $y \in \mathbb{R}^{\tilde{d}}$ . In the case that  $X$  and  $Y$  have a joint density, this can be done by Bayes' theorem, which states that

$$p_{X|Y=y}(x) = \frac{p_{Y|X=x}(y)p_X(x)}{p_Y(y)}.$$

Under the assumption that  $y$  is fixed, the term  $p_Y(y)$  is just a constant, such that  $p_{X|Y=y}$  is (up to a multiplicative constant) given by the product of the likelihood  $p_{Y|X=x}(y)$  and the prior  $p_X(x)$ . Figure 7.7 illustrates the prior density  $p_X$  on the left and the posterior density  $p_{X|Y=y}$  for  $y = 0$  on the right for the inverse problem (18) with  $F(x_1, x_2) = x_2$  and  $\eta \sim \mathcal{N}(0, 0.1^2)$ . It can be seen that the observation  $Y = y$  modifies the density  $p_X$  such that the distribution  $p_{X|Y=y}$  is concentrated around the pre-image  $F^{-1}(\{y\})$ . In the literature, the problem of recovering the posterior distribution  $P_{X|Y=y}$  was tackled by MCMC methods in [51] and conditional normalizing flows in [2, 5, 14, 63] or conditional VAEs in [55]. In the following, we show similarly as before that conditional SNFs include all these methods. We are also aware of the concept of conditional GANs [43]. However, as we are not sure how they are related to SNFs, we do not consider them in detail.

### 7.1. Conditional Normalizing Flows

A conditional normalizing flow is a mapping  $\mathcal{T} = \mathcal{T}_\theta: \mathbb{R}^{\tilde{d}} \times \mathbb{R}^d \rightarrow \mathbb{R}^d$  such that for any  $y \in \mathbb{R}^{\tilde{d}}$ , the function  $\mathcal{T}(y, \cdot)$  is invertible. Here, we call  $y$  the *condition* of  $\mathcal{T}(y, \cdot)$ . Then, it can be used

to model the density  $p_{X|Y=y}$  of  $P_{X|Y=y}$  for an arbitrary  $y \in \mathbb{R}^{\tilde{d}}$  by a simpler distribution  $P_Z$ , by learning  $\mathcal{T}$  such that it holds approximately

$$P_{X|Y=y} \approx \mathcal{T}(y, \cdot)_{\#} P_Z, \quad \text{or equivalently} \quad P_Z \approx \mathcal{T}(y, \cdot)_{\#}^{-1} P_X.$$

Similarly as in the non-conditional case this approximation can be done by the expected Kullback-Leibler divergence

$$\begin{aligned} & \mathbb{E}_{y \sim P_Y} [\text{KL}(P_{X|Y=y}, \mathcal{T}(y, \cdot))] \\ &= \mathbb{E}_{y \sim P_Y} \left[ \mathbb{E}_{x \sim P_{X|Y=y}} \left[ \log \left( \frac{p_{X|Y=y}(x)}{p_{\mathcal{T}(y, \cdot)_{\#} P_Z}(x)} \right) \right] \right] \\ &= \mathbb{E}_{(x, y) \sim P_{X, Y}} [p_{X|Y=y}] - \mathbb{E}_{(x, y) \sim P_{X, Y}} \left[ \log (p_Z \circ \mathcal{T}^{-1}(y, x)) \right. \\ & \quad \left. + \log |\det(\nabla \mathcal{T}^{-1}(y, x))| \right], \end{aligned}$$

where  $\mathcal{T}^{-1}(y, x)$  is the function  $\mathcal{T}^{-1}(y, \cdot)$  evaluated at  $x$  and  $\nabla \mathcal{T}^{-1}(y, x)$  denotes its Jacobian. As the first summand is constant, we obtain the loss function

$$\mathcal{L}_{\text{cNF}}(\theta) := -\mathbb{E}_{(x, y) \sim P_{X, Y}} \left[ \log (p_Z \circ \mathcal{T}^{-1}(y, x)) + \log |\det(\nabla \mathcal{T}^{-1}(y, x))| \right].$$

Now, let  $\mathcal{T}$  be the composition of multiple blocks, i.e.,

$$\mathcal{T}(y, \cdot) = \mathcal{T}_T(y, \cdot) \circ \cdots \circ \mathcal{T}_1(y, \cdot).$$

Then, the blocks generate two sequences  $(X_0, \dots, X_T)$  and  $(Y_T, \dots, Y_0)$  of random variables

$$X_0 \sim P_Z, \quad X_t = \mathcal{T}_t(Y, X_{t-1}) \quad \text{and} \quad Y_T = X, \quad Y_{t-1} = \mathcal{T}_t^{-1}(Y, Y_t).$$

Due to the condition, it is now intractable to compute the kernels  $P_{X_t|X_{t-1}}$  and  $P_{Y_{t-1}|Y_t}$ . Instead, we consider the kernels  $\mathcal{K}_t = P_{X_t|X_{t-1}, Y}$  and  $\mathcal{R}_t = P_{Y_{t-1}|Y_t, Y}$ . By a similar computation as in the non-conditional case, they are given by

$$\mathcal{K}_t(y, x, \cdot) = \delta_{\mathcal{T}_t(y, x)} \quad \text{and} \quad \mathcal{R}_t(y, x, \cdot) = \delta_{\mathcal{T}_t^{-1}(y, x)}.$$

Note, that for an arbitrary  $y$  the distributions  $P_{(X_0, \dots, X_T)|Y=y}$  and  $P_{(Y_T, \dots, Y_0)|Y=y}$  are determined by

$$P_Z \times \mathcal{K}_1(y, \cdot, \cdot) \times \cdots \times \mathcal{K}_T(y, \cdot, \cdot) \quad \text{and} \quad P_{X|Y=y} \times \mathcal{R}_T(y, \cdot, \cdot) \times \cdots \times \mathcal{R}_1(y, \cdot, \cdot)$$

such that any two sequences  $(X_0^y, \dots, X_T^y)$  and  $(Y_T^y, \dots, Y_0^y)$  following these distributions are Markov chains.

## 7.2. Conditional SNFs

As in the non-conditional case, we obtain conditional SNFs from conditional normalizing flows by replacing some of the deterministic transitions  $\mathcal{T}_t$  by random transforms. In terms of Markov kernels, we replace the Dirac measures from  $\mathcal{K}_t$  and  $\mathcal{R}_t$  by more general kernels. This leads to the following formal definition of conditional SNFs. A *conditional SNF* is a pair of sequences  $((X_0, \dots, X_T), (Y_T, \dots, Y_0))$  of random variables  $X_t, Y_t : \Omega \rightarrow \mathbb{R}^{d_t}$  such that:

cP1) the conditional distributions  $P_{X_t|Y=y}$  and  $P_{Y_t|Y=y}$  have densities

$$p_{X_t}(y, \cdot) : \mathbb{R}^{d_t} \rightarrow \mathbb{R}_{>0}, \quad \text{and} \quad p_{Y_t}(y, \cdot) : \mathbb{R}^{d_t} \rightarrow \mathbb{R}_{>0}$$

for  $P_Y$ -almost every  $y$  and all  $t = 1, \dots, T$ ,

cP2) for  $P_Y$ -almost every  $y$ , there exist Markov kernels  $\mathcal{K}_t : \mathbb{R}^{\tilde{d}} \times \mathbb{R}^{d_{t-1}} \times \mathcal{B}(\mathbb{R}^{d_t}) \rightarrow [0, 1]$  and  $\mathcal{R}_t : \mathbb{R}^{\tilde{d}} \times \mathbb{R}^{d_t} \times \mathcal{B}(\mathbb{R}^{d_{t-1}}) \rightarrow [0, 1]$  such that

$$\begin{aligned} P_{(X_0, \dots, X_T)|Y=y} &= P_{X_0} \times \mathcal{K}_1(y, \cdot, \cdot) \times \dots \times \mathcal{K}_T(y, \cdot, \cdot), \\ P_{(Y_T, \dots, Y_0)|Y=y} &= P_{Y_0} \times \mathcal{R}_T(y, \cdot, \cdot) \times \dots \times \mathcal{R}_1(y, \cdot, \cdot). \end{aligned}$$

cP3) for  $P_{Y, X_t}$ -almost every pair  $(y, x) \in \mathbb{R}^{\tilde{d}} \times \mathbb{R}^{d_t}$ , the measures  $\mathcal{R}_t(y, x, \cdot)$  and  $P_{X_{t-1}|X_t=x, Y=y}(\cdot)$  are absolute continuous with respect to each other.

We call the sequence  $(Y_T, \dots, Y_0)$  a *reverse* of  $(X_0, \dots, X_T)$ . For applications, one usually sets

$$X_0 = Z,$$

where  $Z$  is a random variable, which is easy to sample from and we aim to approximate for any  $y \in \mathbb{R}^{\tilde{d}}$  the distribution  $P_{X|Y=y}$  by  $P_{X_T|Y=y}$ . On the other hand, the reverse usually starts with

$$P_{Y_T|Y=y} = P_{X|Y=y}$$

and  $P_{Y_0}$  should approximate the latent distribution  $P_Z$ .

The stochastic layers can be chosen analogously as in the non-conditional case. For details, we refer to [24].

For training conditional SNFs, we aim to minimize the Kullback-Leibler divergence

$$\text{KL}(P_{Y, (Y_0, \dots, Y_T)}, P_{Y, (X_0, \dots, X_T)}).$$

By [24, Corollary 9], this is equivalent to minimizing

$$\begin{aligned} \mathcal{L}_{\text{cSNF}}(\theta) &= \mathbb{E}_{y \sim P_Y} \left[ \mathbb{E}_{(x_0, \dots, x_T) \sim P_{Y_0^y, \dots, Y_T^y}} \left[ \right. \right. \\ &\quad \left. \left. \log \left( \frac{1}{p_Z(x_0)} \prod_{t=1}^T \frac{f_{t,y}(x_{t-1}, x_t) p_{X_{t-1}^y}(x_{t-1})}{p_{X_t^y}(x_t)} \right) \right] \right], \end{aligned}$$

where  $f_{t,y}(\cdot, x_t)$  is given by the Radon-Nikodym derivative  $\frac{dP_{Y_{t-1}^y|Y_t^y=x_t}}{dP_{X_{t-1}^y|X_t^y=x_t}}$  and where the pair  $((X_0^y, \dots, X_T^y), (Y_T^y, \dots, Y_0^y))$  of Markov chains follows the distributions

$$P_Z \times \mathcal{K}_1(y, \cdot, \cdot) \times \dots \times \mathcal{K}_T(y, \cdot, \cdot) \quad \text{and} \quad P_X \times \mathcal{R}_T(y, \cdot, \cdot) \times \dots \times \mathcal{R}_1(y, \cdot, \cdot).$$

**Example 7.1.** Once a conditional (stochastic) normalizing flow is trained, we can reconstruct the posterior distribution  $P_{X|Y=y}$  for any observation  $y$ . In particular, this allows us to interpolate between the posterior distributions  $P_{X|Y=y_0}$  and  $P_{X|Y=y_1}$  by the distributions  $P_{X|Y=y}$  for  $y = (1 - \lambda)y_0 + \lambda y_1$ . We plot the one dimensional marginals of such an interpolation for the example from Section 8.2 in Figure 7.8.

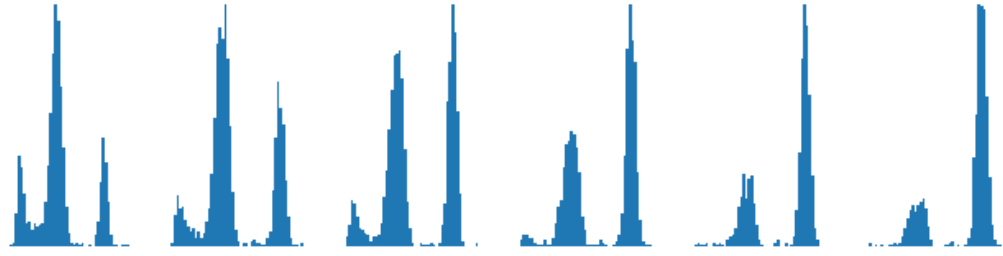


Figure 7.8: One dimensional marginals of the interpolations  $P_{X|Y=y}$  with  $y = (1 - \lambda)y_0 + \lambda y_1$  between the posterior distributions  $P_{X|Y=y_0}$  and  $P_{X|Y=y_1}$  using equidistant  $\lambda \in [0, 1]$  for the inverse problem from Section 8.2.

### 7.3. Conditional VAEs

The authors of [55] proposed conditional VAEs. A *conditional VAE* is a pair  $(E, D)$  of a conditional stochastic decoder

$$D(y, z) = D_\theta(y, z) := (\mu_\theta(y, z), \Sigma_\theta(y, z))$$

and a conditional stochastic encoder

$$E(y, x) = E_\phi(y, x) := (\mu_\phi(y, x), \Sigma_\phi(y, x)).$$

The networks  $E$  and  $D$  are learned such that the kernels

$$\begin{aligned} \mathcal{K}(y, z, \cdot) &:= \mathcal{N}(\mu_\theta(y, z), \Sigma_\theta(y, z)), \\ \mathcal{R}(y, x, \cdot) &:= \mathcal{N}(\mu_\phi(y, x, \cdot), \Sigma_\phi(y, x, \cdot)) \end{aligned}$$

push the probability distribution  $P_Z$  onto  $P_{X|Y=y}$  and vice versa. As a loss function, a straight forward modification of the ELBO (12) is used. Similar, as in the non-conditional case, it turns out that a conditional VAE is a one-layer conditional SNF with layers  $\mathcal{K}$  and  $\mathcal{R}$  as defined above.

## 8. Numerical Results

In this section, we show two numerical examples. The first one with Gaussian mixture models is academical, but quite useful, since we know the ground truth and can give quantitative comparisons. The second example is a real world example from scatterometry. Both setups were also used in [24], but the models and comparisons are different.

### 8.1. Posterior Approximation for Gaussian Mixtures

To verify that our proposed methods yield the correct posteriors, we apply our framework to a linear inverse problem with a Gaussian mixture model, where we can analytically infer the ground truth by the following lemma, which can also be found in [24].

**Lemma 8.1.** Let  $X \sim \sum_{k=1}^K w_k \mathcal{N}(m_k, \Sigma_k)$ . Suppose that

$$Y = AX + \eta,$$

where  $A : \mathbb{R}^d \rightarrow \mathbb{R}^{\tilde{d}}$  is a linear operator and we have Gaussian noise  $\eta \sim N(0, b^2 I)$ . Then

$$P_{X|Y=y} \propto \sum_{k=1}^K \tilde{w}_k \mathcal{N}(\cdot | \tilde{m}_k, \tilde{\Sigma}_k),$$

where  $\propto$  denotes equality up to a multiplicative constant and

$$\tilde{\Sigma}_k := (\frac{1}{b^2} A^T A + \Sigma_k^{-1})^{-1}, \quad \tilde{m}_k := \tilde{\Sigma}_k (\frac{1}{b^2} A^T y + \Sigma_k^{-1} m_k).$$

and

$$\tilde{w}_k := \frac{w_k}{|\Sigma_k|^{\frac{1}{2}}} \exp \left( \frac{1}{2} (\tilde{m}_k \tilde{\Sigma}_k^{-1} \tilde{m}_k - m_k \Sigma_k^{-1} m_k) \right).$$

*Proof.* First, consider one component  $P_{X_k} = \mathcal{N}(m_k, \Sigma_k)$ . Using Bayes' theorem we get

$$\begin{aligned} p_{X_k|Y_k=y}(x) &= p_{Y_k|X_k=x}(y) p_{X_k}(x) / p_{Y_k}(y), \\ p_{Y_k}(y) &= \int_{\mathbb{R}^{\tilde{d}}} p_{X_k}(z) p_{Y_k|X_k=z}(y) dz \end{aligned}$$

and further

$$\begin{aligned} p_{Y_k|X_k=x}(y) p_{X_k}(x) &= \mathcal{N}(y | Ax, b^2 I) \mathcal{N}(x | m_k, \Sigma_k) \\ &\propto \frac{1}{|\Sigma_k|^{\frac{1}{2}}} \exp \left( -\frac{1}{2} (x - \tilde{m}_k)^T \tilde{\Sigma}_k^{-1} (x - \tilde{m}_k) \right) \exp \left( -\frac{1}{2} m_k^T \Sigma_k^{-1} m_k + \frac{1}{2} \tilde{m}_k^T \tilde{\Sigma}_k^{-1} \tilde{m}_k \right) \end{aligned}$$

with a constant independent of  $k$ . Then we get for the mixture model  $P_X \sim \sum_{k=1}^K w_k \mathcal{N}(m_k, \Sigma_k)$  again by Bayes' theorem that

$$\begin{aligned} p_{X|Y=y}(x) &\propto \sum_{k=1}^K w_k p_{Y|X=x}(y) \mathcal{N}(x | m_k, \Sigma_k) \\ &\propto \sum_{k=1}^K \frac{w_k}{|\Sigma_k|^{\frac{1}{2}}} \exp \left( -\frac{1}{2} (x - \tilde{m}_k)^T \tilde{\Sigma}_k^{-1} (x - \tilde{m}_k) \right) \exp \left( -\frac{1}{2} m_k^T \Sigma_k^{-1} m_k + \frac{1}{2} \tilde{m}_k^T \tilde{\Sigma}_k^{-1} \tilde{m}_k \right) \\ &\propto \sum_{k=1}^K \tilde{w}_k \mathcal{N}(\cdot | \tilde{m}_k, \tilde{\Sigma}_k). \end{aligned}$$

□

In our experiment, we consider the Gaussian mixture model on  $\mathbb{R}^{100}$  given by

$$X \sim \sum_{k=1}^5 \frac{1}{5} \mathcal{N}(m_k, \Sigma_k), \quad \Sigma_k = 10^{-4} I,$$

where the means were chosen uniformly in the interval  $[-1, 1]$ . As operator  $A$  we use the diagonal matrix with entries  $a_{i,i} = 0.1/(i+1)^2$ . Finally, we choose  $b = 0.05$  for the Gaussian noise  $\eta$ . Note that the variance of the mixture components was chosen very small, so that the posterior is very concentrated around its modes. This makes the problem particularly challenging and underpins the need for stochastic layers. Furthermore, the dimension 100 of this problem is quite large for Bayesian inversion.

We test the following 6 conditional models, which all have a similar number of parameters ranging from 779840 to 882240. All were trained for 5000 iterations, where the pure VAE model trained the quickest. The slowest to train was the INN with MALA model, which took a little bit more than a factor of 2 of the VAE model.

In the following, we give a more accurate description of the used models. When we speak of VAEs we mean layers of the form  $\mathcal{K}(y, x, \cdot) = \mathcal{N}(f(y, x), \sigma^2 I)$  and  $\mathcal{R}(y, x, \cdot) = \mathcal{N}(g(y, x), \sigma^2 I)$  for some neural networks  $f$  and  $g$ , i.e. we choose the fixed covariance matrix  $\sigma^2 I$  within the stochastic decoder and encoder. Note that the quotient in the loss for the VAE layer in Lemma 6.4 enforces that the networks  $f$  and  $g$  are "approximately inverse" to each other.

- **INN:** Here we took 8 coupling layers with a subnetwork with 2 hidden layers containing 128 neurons in them.
- **VAE:** They consist of a forward and backward ReLU neural network with 2 hidden layers of size 128. We concatenated 8 layers of them, with noise levels of 0.1 and a noise level of 0.01 in the final layer.
- **INN and VAE:** Here we took 4 layers, which consisted of one coupling and one autoencoder as above. Furthermore, in the final layer we used noise level 0.01.
- **MALA and INN:** Same architecture as the conditional INN and a MALA layer in the last layer. The MALA layer uses 3 Metropolis–Hastings steps with step size of 5e-5.
- **MALA and VAE:** Same architecture as the autoencoder (8 layers with noise level of 0.1) with a MALA layer as the final layer.
- **MALA and VAE and INN:** Same architecture as the conditional INN and autoencoder, but with a MALA layer as the final layer.

Furthermore, we evaluated the average Wasserstein-1 distance of the posteriors compared to the ground truth. For this, we trained all models 5 times and averaged the Wasserstein-1 distance over 100 independently drawn values of  $y$ . We obtained the following results:

Method	INN	INN+MALA	VAE	VAE+INN	VAE+MALA	INN+VAE+MALA
$W_1$	3.55	2.92	1.22	1.18	0.8	0.82

We observed that VAE+MALA worked best, but INN+VAE+MALA was only slightly worse. The models VAE and VAE+INN performed comparatively. The conditional INN+MALA were much worse, but better than the conditional INN.

The results are depicted in Figure 8.9 and 8.10. This numerical evaluation shows in particular that combining different kinds of layers will certainly be helpful when modeling densities: The

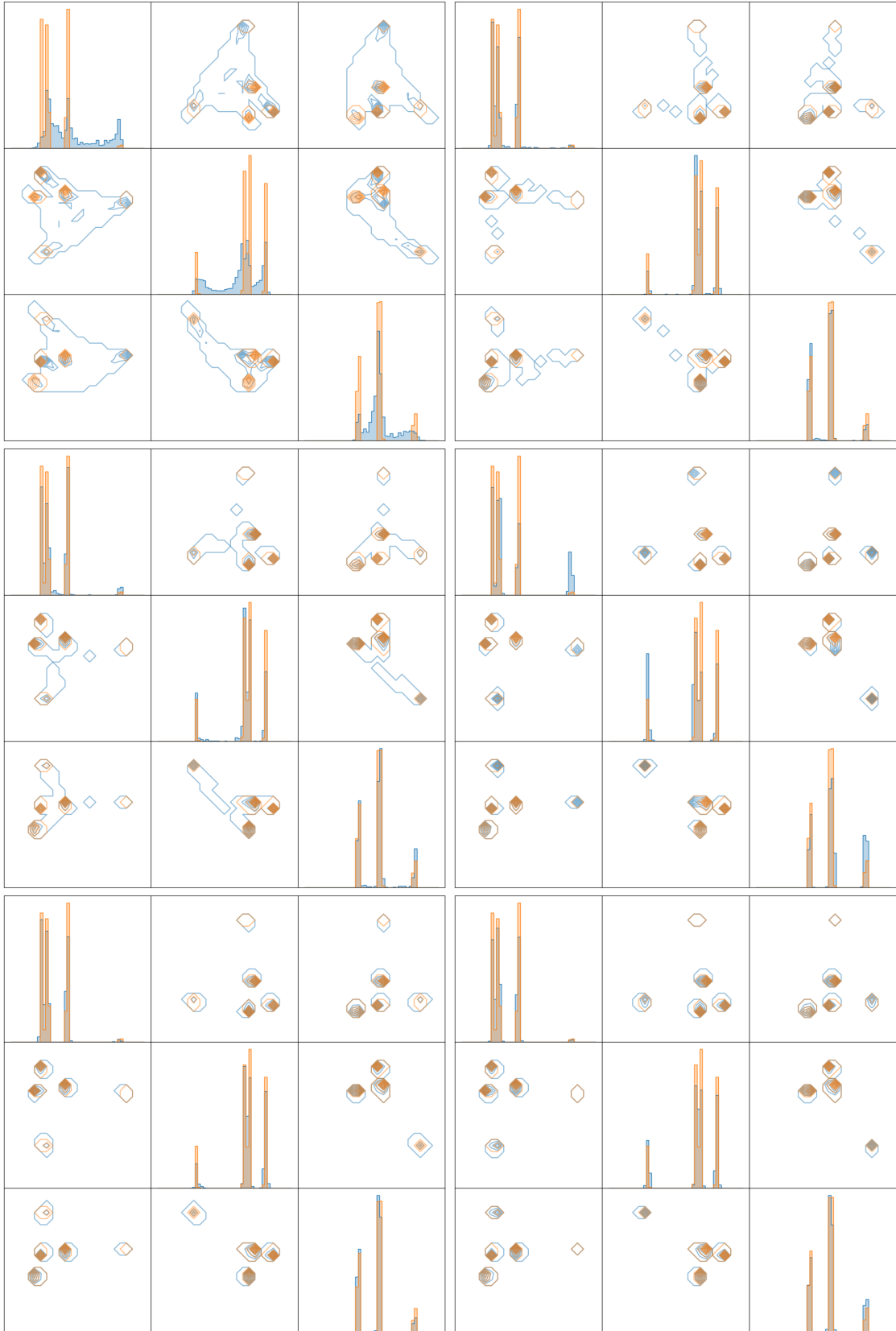


Figure 8.9: Histograms and 2-marginals of the first, 50-th and 100-th marginal of the ground truth (orange) and the posterior reconstructions of the six different models. Row-wise from upper left to lower right: INN, INN + MALA, VAE, INN + VAE, VAE+MALA, INN+VAE+MALA

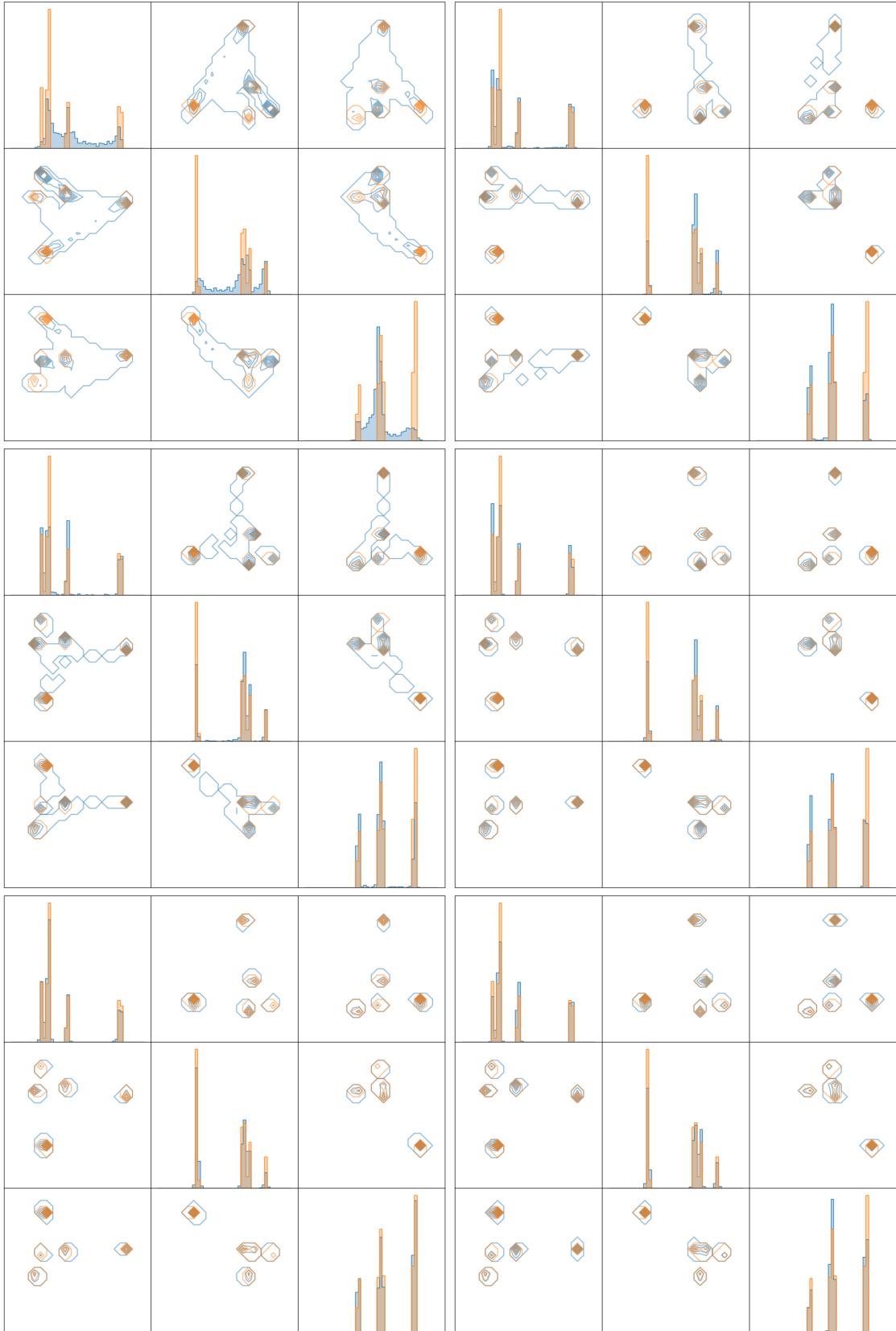


Figure 8.10: Histograms and 2-marginals of the first, 50-th and 100-th marginal of the ground truth (orange) and the posterior reconstructions of the six different models. Row-wise from upper left to lower right: INN, INN + MALA, VAE, INN + VAE, VAE+MALA, INN+VAE+MALA

MALA layer seems to help to anneal to the exact peaks whereas the pure INN models seem to smear those peaks out, as can be seen in the top left and right of the two figures. However, inserting a MALA layer only in the last layer of INNs does not yield very good results, as the MALA layer has trouble with the mixing of different modes, i.e. the mass does not seem to be distributed perfectly. Furthermore, the variational autoencoder seems to be better at modeling those peaky densities themselves. However note that we did not optimize model parameters that much. For instance, learning proposals or learning the covariance of autoencoders can certainly help to obtain better results. We however followed the rough intuition, that we want to decrease the noise level in the last layer so that we have a chance to model the distribution correctly.

## 8.2. Example from Scatterometry

In this example, we are concerned with a non-destructive technique to determine the structures of photo masks described in more detail in [29, 30]. Here  $F: \mathbb{R}^3 \rightarrow \mathbb{R}^{23}$  is a nonlinear forward operator which describes the diffraction of monochromatic lights on line gratings. The parameters in  $x$ -space describe the geometry of the line gratings and

$$Y = F(X) + \eta$$

the diffraction pattern. The inverse problem consists in recovering the geometry given an observation  $y$ . We assume that the noise  $\eta$  is mixed additive and multiplicative Gaussian noise, i.e.,  $\eta = aF(X)\eta_1 + b\eta_2$ , where  $\eta_1, \eta_2 \sim \mathcal{N}(0, I)$  and  $a, b > 0$  are some constants. Then, the conditional distribution  $P_{Y|X=x}$  is given by  $\mathcal{N}(F(x), (a^2F(x)^2 + b^2)I)$ . Here  $b$  represents the strength of background noise, while  $a$  controls the strength of fluctuations depending on the forward model. In our experiment we can assume that  $a = 0.2$  and  $b = 0.01$ .

In scatterometry, the forward operator  $F$  is known from physics, but its evaluation requires the solution of some partial differential equation, see [30], which is slow and computationally costly. We approximated this forward operator using a simple feed forward neural network.

Since we do not have any prior information about the parameters  $x$ , we choose the prior distribution  $P_X$  as the uniform distribution on  $[-1, 1]^3$ . For the conditional SNF we assumed that  $P_X$  has a strictly positive density  $p_X$ . To fulfill this assumption, we relax the probability density function of the uniform distribution for  $x = (x_1, x_2, x_3) \in \mathbb{R}^3$  by

$$p_X(x) := q(x_1)q(x_2)q(x_3),$$

where

$$q(x) := \begin{cases} \frac{\alpha}{2\alpha+2} \exp(-\alpha(-1-x)), & \text{for } x < -1, \\ \frac{\alpha}{2\alpha+2}, & \text{for } x \in [-1, 1], \\ \frac{\alpha}{2\alpha+2} \exp(-\alpha(x-1)), & \text{for } x > 1, \end{cases}$$

and  $\alpha \gg 0$  is some constant. In our numerical experiments, we choose  $\alpha = 1000$ .

We repeat the numerical experiment from the previous section with less models. In particular, we use the following models with a similar number of parameters (roughly 50000) and trained for the same number of epochs, namely 5000. One epoch consists of 8 optimizer steps. Note that using a MALA layer increases computational effort (roughly by a factor of 2). We used a batch size of 1600.

- **INN**: We use 4 layers with 64 hidden neurons, where each feedforward neural network has two hidden layers.
- **INN+MALA**: The same architecture, but with a MALA layer with step size 5e-3 and 3 steps in the last layer.
- **VAE**: Here we use standard ReLU feedforward neural networks with hidden size 64, and 4 layers of them.
- **VAE+MALA**: Same architecture with a MALA layer with step size 5e-3 and 3 steps.

Similar to [24], we obtain the "ground truth" posterior samples via MCMC, where we apply the Metropolis–Hastings kernel 1000 times with a uniform initialization.

We obtained the following averaged KL-distances  $\text{KL}(\mu_{MCMC}, \mu_{SNF})$  (where we approximated the empirical measures via histograms). Results are averaged over 3 training runs, where in each the KL distance is approximated using 20 samples from  $P_Y$ .

Method	INN	INN+MALA	VAE	VAE+MALA
$KL$	0.76	0.59	0.98	0.69

In the figures 8.11 and 8.12 one can see exemplary posterior plots comparing the different methods. Basically one can see that the MALA layer improves mass distribution, often removing unnecessary mass from low density regions. Furthermore, the distribution of mass seems best for the INN MALA combination, confirming quantitative results.

### 8.3. Image generation via 2d energy modeling

Suppose we are given two images  $\mu_0$  and  $\mu_1$  of smileys considered as discrete measures on the image grid with the associated gray values as weights. There are many viable ways to interpolate them. A natural one uses Wasserstein-2 barycenters resulting in the McCann interpolation

$$\mu_t = ((1-t)\text{id} + tT)_{\mu_0},$$

where  $T$  denotes the optimal transport map between  $\mu_0$  and  $\mu_1$ . As condition we use a path  $(\mu_t)_t$  between two smileys for equispaced values of  $t$  in  $[0, 1]$ . With this at hand, we are finally able to train both a conditional SNF as well as a conditional INN on these smileys. The results are shown in Figure 8.13, where the top row shows samples of the conditional SNF and the bottom row shows samples of the conditional INN. Both have the same number of parameters and were trained for roughly the same time. However the conditional SNF has more information as we use MCMC layers in between INN layers, which need to evaluate the densities. The conditional INN only requires samples for learning. That being said, the conditional SNF does a much better job at recovering those concentrated 2d densities, as MH layers are able to move the mass from low density regions quite efficiently by jumping. On the other hand, the conditional INN clearly captures the shape, but the details get blurred out.

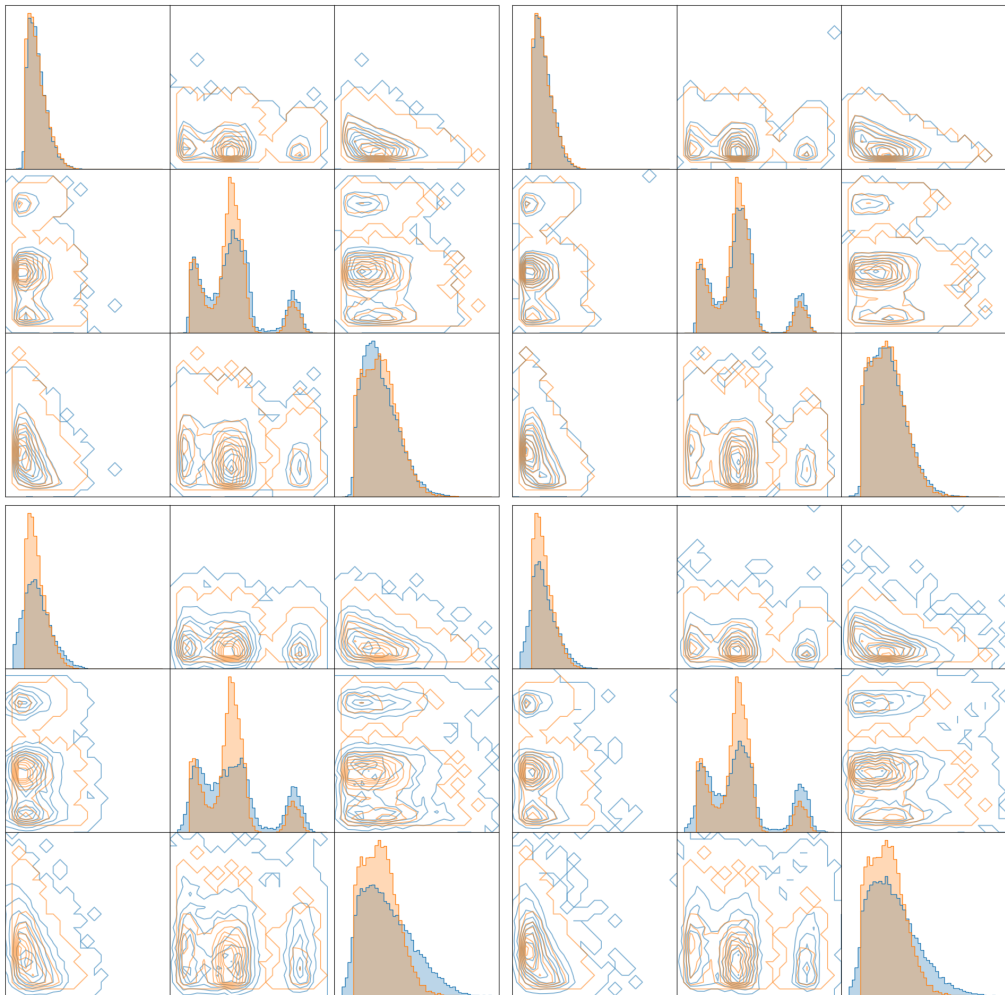


Figure 8.11: Histograms of the posterior reconstructions using a different SNF methods in blue and MCMC in orange for one sample from  $Y$ . In the upper left, there is the INN, upper right there is the INN+MALA, then in the lower left the VAE follows and in the lower right the VAE+MALA model follows. On the diagonal we plot the histograms of the one-dimensional marginals, on the off-diagonal we plot the distributions of the two dimensional marginals.

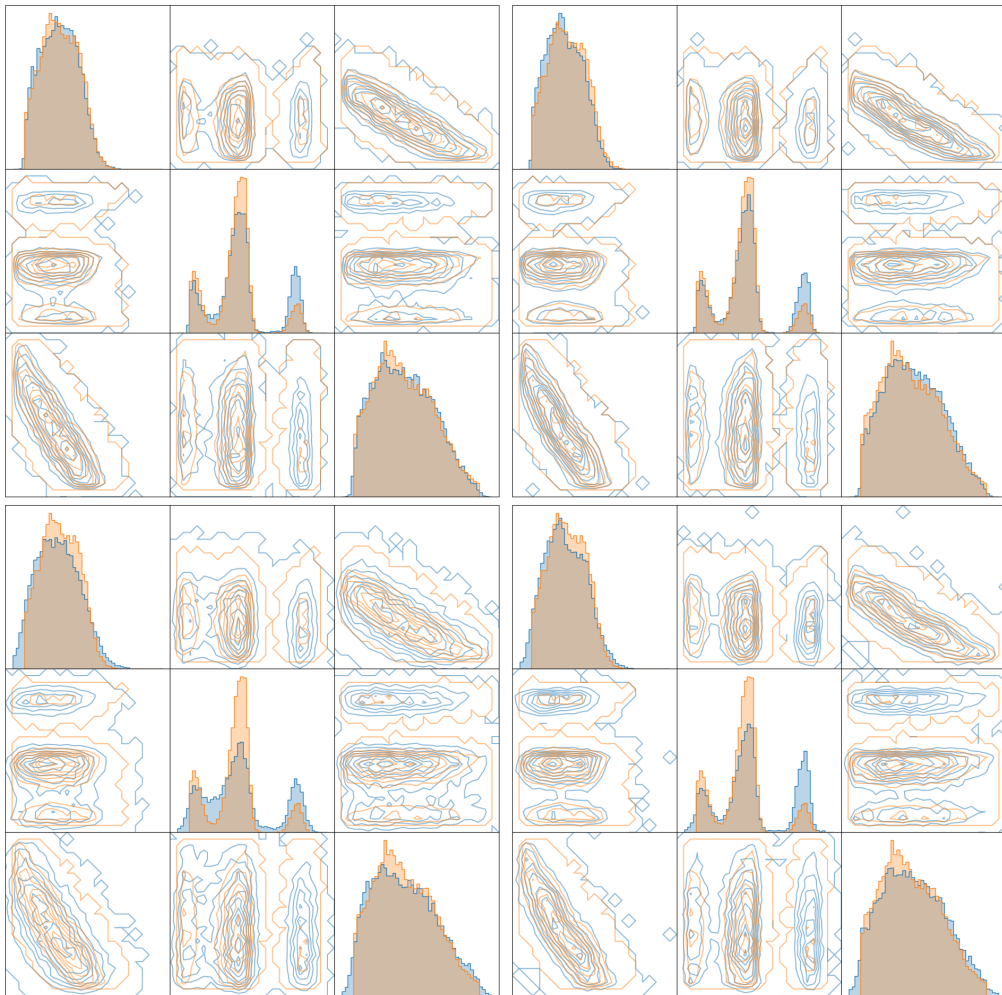


Figure 8.12: Histograms of the posterior reconstructions using a different SNF methods in blue and MCMC in orange for one sample from  $Y$ . In the upper left, there is the INN, upper right there is the INN+MALA, then in the lower left the VAE follows and in the lower right the VAE+MALA model follows. On the diagonal we plot the one histograms of the one-dimensional marginals, on the off-diagonal we plot the potentials of the two dimensional marginals.

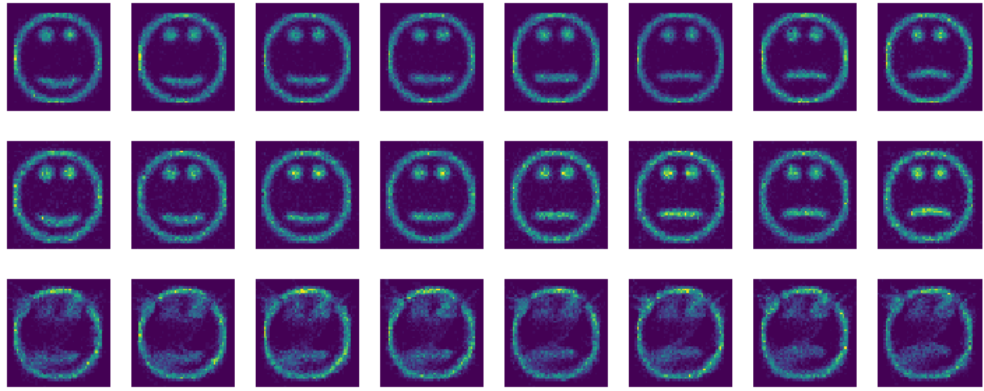


Figure 8.13: Modeling of smileys as 2d densities with true samples (top row), conditional SNF (middle row) and conditional INN (bottom row)

## A. Invertible Neural Networks

Invertible neural networks  $\mathcal{T} = \mathcal{T}(\cdot; \theta)$  with parameters  $\theta$ , which can be used in finite normalizing flows, are compositions

$$\mathcal{T} = T_L \circ P_L \circ \cdots \circ T_1 \circ P_1, \quad (19)$$

of permutation matrices  $P_\ell$  and diffeomorphisms  $T_\ell$ ,  $\ell = 1, \dots, L$ , i.e.,  $T_\ell$  are bijections and both  $T_\ell$  and  $T_\ell^{-1}$  are continuously differentiable. There are mainly two ways to create such invertible mappings, namely as

- residual neural networks (ResNets) and
- directly invertible neural networks (INNs).

In the following, we briefly explain these architectures, where we fix the index and refer just to  $T$  instead of  $T_\ell$ .

### A.1. ResNets

Invertible Residual Networks were introduced in [6] and applied to various problems, see [8, 7]. Here  $T$  has the structure

$$T(x) = x + \Phi(x; \theta), \quad (20)$$

where  $\Phi(x; \theta)$  is a Lipschitz continuous subnetwork with Lipschitz constant smaller than 1. Then given  $y = T(x) = x + \Phi(x; \theta)$ , the inversion of (20) can be done by considering the fixed point equation

$$x = y - \Phi(x; \theta)$$

and applying the Picard iteration

$$\begin{aligned} x^{(0)} &= y, \\ \text{For } r &= 0, 1, \dots \\ x^{(r+1)} &= y - \Phi(x^{(r)}; \theta). \end{aligned}$$

By Banach's fixed point theorem the sequence  $\{x^{(r)}\}_r$  converges to  $T^{-1}(y)$ . In general, much effort needs to be invested in order to control the Lipschitz constant of the subnetworks in the learning process and several variants were proposed by the above authors. An alternative would be to restrict the networks  $\Phi(x; \theta)$  to so-called proximal neural networks which are automatically averaged operators having a Lipschitz constant not larger than one. Such networks were proposed based on a paper of [9] in [26, 32]. But clearly, „there is no free lunch” and the learning process of a proximal neural networks requires a stochastic gradient descent algorithm on a Stiefel manifold which is more expensive than the algorithm in the Euclidean space. For another approach, we refer to [48].

## A.2. INNs

In INNs, the networks  $T$  are directly invertible due to their special structure, namely either a simple triangular one or a slightly more sophisticated block exponential one. We briefly sketch the triangular structure and explain in more detail the second model, since this is used in our numerical examples.

Real-valued volume-preserving transformations (real NVPs) were introduced in [15]. They have the form

$$T(\xi_1, \xi_2) := \begin{pmatrix} \xi_1 \\ \xi_2 e^{s(\xi_1)} + t(\xi_1) \end{pmatrix}, \quad \xi = \begin{pmatrix} \xi_1 \\ \xi_2 \end{pmatrix} \in \mathbb{R}^d,$$

where  $\xi_1 \in \mathbb{R}^{d_1}$ ,  $\xi_2 \in \mathbb{R}^{d_2}$  and  $d = d_1 + d_2$ . Here  $s, t : \mathbb{R}^{d_2} \rightarrow \mathbb{R}^{d_1}$  are subnetworks and the product and exponential are taken componentwise. Then the inverse map is obviously

$$T(x_1, x_2) := \begin{pmatrix} x_1 \\ (x_2 - t(x_1)) e^{-s(x_1)} \end{pmatrix}, \quad x = \begin{pmatrix} x_1 \\ x_2 \end{pmatrix} \in \mathbb{R}^d.$$

and does not require an inversion of the feed-forward subnetworks. Hence the whole map  $\mathcal{T}$  is invertible and allows for a fast evaluation of both forward and inverse map.

In our experiments, we use the slightly sophisticated architecture proposed in [4, 2] which has the form

$$T(\xi_1, \xi_2) = (x_1, x_2) := \begin{pmatrix} \xi_1 e^{s_2(\xi_2)} + t_2(\xi_2) \\ \xi_2 e^{s_1(x_1)} + t_1(x_1) \end{pmatrix}, \quad \xi = \begin{pmatrix} \xi_1 \\ \xi_2 \end{pmatrix} \in \mathbb{R}^d$$

for some splitting  $(\xi_1, \xi_2) \in \mathbb{R}^d$  with  $\xi_i \in \mathbb{R}^{d_i}$ ,  $i = 1, 2$ . Here  $s_2, t_2 : \mathbb{R}^{d_2} \rightarrow \mathbb{R}^{d_1}$  and  $s_1, t_1 : \mathbb{R}^{d_1} \rightarrow \mathbb{R}^{d_2}$  are ordinary feed-forward neural networks. The parameters  $\theta$  of  $\mathcal{T}(\cdot; \theta)$  are specified by the parameters of these subnetworks. The inverse of the network layers  $T$  is

$$T^{-1}(x_1, x_2) = (\xi_1, \xi_2) := \begin{pmatrix} (x_1 - t_2(\xi_2)) e^{-s_2(\xi_2)} \\ (x_2 - t_1(x_1)) e^{-s_1(x_1)} \end{pmatrix}.$$

In our loss function of the form (5), we will need the log-determinant of  $\mathcal{T}$  in (19). Fortunately this can be simply computed by the following considerations: since  $T_\ell = T_{2,\ell} \circ T_{1,\ell}$  with

$$\begin{aligned} T_{1,\ell}(\xi_1, \xi_2) &= (x_1, \xi_2) := \left( \xi_1 e^{s_{\ell,2}(\xi_2)} + t_{\ell,2}(\xi_2), \xi_2 \right), \\ T_{2,\ell}(x_1, \xi_2) &= (x_1, x_2) := \left( x_1, \xi_2 e^{s_{\ell,1}(x_1)} + t_{\ell,1}(x_1) \right), \end{aligned}$$

we have

$$\nabla T_{1,\ell}(\xi_1, \xi_2) = \begin{pmatrix} \text{diag}(e^{s_{\ell,2}(\xi_2)}) & \text{diag}(\nabla_{\xi_2}(\xi_1 e^{s_{\ell,2}(\xi_2)} + t_{\ell,2}(\xi_2))) \\ 0 & I_{d_2} \end{pmatrix}$$

so that  $\det \nabla T_{1,\ell}(\xi_1, \xi_2) = \prod_{k=1}^{d_1} e^{(s_{\ell,2}(\xi_2))_k}$  and similarly for  $\nabla T_{2,\ell}$ . Applying the chain rule in (19) and noting that the Jacobian of  $P_\ell$  is just  $P_\ell$  with  $|\det P_\ell| = 1$ , and that  $\det(AB) = \det(A)\det(B)$ , we conclude

$$\log(|\det(\nabla \mathcal{T}(\xi))|) = \sum_{\ell=1}^L \left( \sum \left( s_{\ell,2} \left( (P_\ell \xi^\ell)_2 \right) \right) + \sum \left( s_{\ell,1} \left( (T_{1,\ell} P_\ell \xi^\ell)_1 \right) \right) \right),$$

where sum denotes the sum of the components of the respective vector,  $\xi^1 := \xi$  and  $\xi^\ell = T_{\ell-1} P_{\ell-1} \xi^{\ell-1}$ ,  $\ell = 2, \dots, L$ .

## B. Auxiliary Results

**Lemma B.1.** *Let  $(X_0, \dots, X_T)$  be a Markov chain. Then  $(X_T, \dots, X_0)$  is again a Markov chain.*

*Proof.* Using that for  $l = T, \dots, 0$  it holds

$$P_{(X_l, \dots, X_T)} = P_{(X_l, X_{l+1})} \times P_{X_{l+2}|X_{l+1}=\cdot} \times \dots \times P_{X_T|X_{l-1}=\cdot}$$

we obtain for any measurable rectangle  $A_{l+1} \times \dots \times A_T$  that

$$\begin{aligned} &P_{(X_T, \dots, X_l)}(A_L \times \dots \times A_l) \\ &= \int_{A_{l+1} \times A_l} \int_{A_{l+2}} \dots \int_{A_{T-1}} P_{X_T|X_{l+1}=x_{l+1}}(A_T) dP_{X_{T-1}|X_{T-2}=x_{T-2}}(x_{T-1}) \\ &\quad \dots dP_{X_{l+2}|X_{l+1}=x_{l+1}}(x_{l+2}) dP_{(X_{l+1}, X_l)}(x_{l+1}, x_l). \end{aligned}$$

Since  $P_{(X_{l+1}, X_l)} = P_{X_{l+1}} \times P_{X_l|X_{l+1}=\cdot}$  and using the definition of  $P_{X_{l+1}} \times P_{X_l|X_{l+1}=\cdot}$ , this is equal to

$$\begin{aligned} &\int_{A_{l+1} \times A_l} \int_{A_{l+2}} \dots \int_{A_{T-1}} P_{X_T|X_{T-1}=x_{T-1}}(A_T) dP_{X_{T-1}|X_{T-2}=x_{T-2}}(x_{T-1}) \\ &\quad \dots dP_{X_{l+2}|X_{l+1}=x_{l+1}}(x_{l+2}) d(P_{X_{l+1}} \times P_{X_l|X_{l+1}=\cdot})(x_{l+1}, x_l) \\ &= \int_{A_{l+1}} \int_{A_{l+2}} \dots \int_{A_{T-1}} P_{X_l|X_{l+1}=x_{l+1}}(A_l) P_{X_T|X_{T-1}=x_{T-1}}(A_T) dP_{X_{T-1}|X_{T-2}=x_{T-2}}(x_{T-1}) \\ &\quad \dots dP_{X_{l+2}|X_{l+1}=x_{l+1}}(x_{l+2}) dP_{X_{l+1}}(x_{l+1}). \end{aligned}$$

By the definition of  $P_{X_{l+1}} \times P_{X_{l+2}|X_{l+1}=\cdot} \times \cdots \times P_{X_T|X_{T-1}=\cdot}$ , this is equal to

$$\begin{aligned}
&= \int_{A_{l+1} \times \cdots \times A_T} P_{X_l|X_{l+1}=x_{l+1}}(A_l) d(P_{X_{l+1}} \times P_{X_{l+2}|X_{l+1}=\cdot} \times \cdots \times P_{X_T|X_{T-1}=\cdot})(x_{l+1}, \dots, x_L) \\
&= \int_{A_{l+1} \times \cdots \times A_T} P_{X_l|X_{l+1}=x_{l+1}}(A_l) dP_{(X_{l+1}, \dots, X_T)}(x_{l+1}, \dots, x_T) \\
&= \int_{A_T \times \cdots \times A_{l+1}} P_{X_l|X_{l+1}=x_{l+1}}(A_l) dP_{(X_L, \dots, X_{l+1})}(x_T, \dots, x_{l+1}) \\
&= P_{(X_T, \dots, X_{l+1})} \times P_{X_l|X_{l+1}=\cdot}(A_T \times \cdots \times A_l)
\end{aligned}$$

Summarizing the above equations yields that

$$P_{(X_T, \dots, X_l)}(A_T \times \cdots \times A_l) = P_{(X_T, \dots, X_{l+1})} \times P_{X_l|X_{l+1}=\cdot}(A_T \times \cdots \times A_l)$$

Since the measurable rectangles are a  $\cap$ -stable generator of the Borel algebra, we obtain that

$$P_{(X_T, \dots, X_l)} = P_{(X_T, \dots, X_{l+1})} \times P_{X_l|X_{l+1}=\cdot}.$$

Using this argument inductively, we obtain that

$$P_{(X_T, \dots, X_0)} = P_{X_T} \times P_{X_{T-1}|X_L=\cdot} \times \cdots \times P_{X_0|X_1=\cdot}.$$

Thus, by the characterization (4),  $(X_T, \dots, X_0)$  is a Markov chain.  $\square$

**Lemma B.2.** *Let  $X, \tilde{X}: \Omega \rightarrow \mathbb{R}^{d_1}$  and  $Y, \tilde{Y}: \Omega \rightarrow \mathbb{R}^{d_2}$  be random variables such that  $X$  and  $Y$  as well as  $\tilde{X}$  and  $\tilde{Y}$  have joint strictly positive densities  $p_{X,Y}$  and  $p_{\tilde{X},\tilde{Y}}$ . Then it holds*

$$\text{KL}(p_X, p_{\tilde{X}}) \leq \text{KL}(p_{X,Y}, p_{\tilde{X},\tilde{Y}}).$$

*Proof.* Using the law of total probability, we obtain

$$\begin{aligned}
\text{KL}(p_X, p_{\tilde{X}}) &= \int_{\mathbb{R}^{d_2}} \int_{\mathbb{R}^{d_1}} p_{X,Y}(x, y) \log\left(\frac{p_{X,Y}(x, y)}{p_{\tilde{X},\tilde{Y}}(x, y)}\right) dx dy \\
&= \int_{\mathbb{R}^{d_2}} \int_{\mathbb{R}^{d_1}} p_X(x) p_{Y|X=x}(y) \left( \log\left(\frac{p_X(x)}{p_{\tilde{X}}(x)}\right) + \log\left(\frac{p_{Y|X=x}(y)}{p_{\tilde{Y}|X=x}(y)}\right) \right) dx dy \\
&= \int_{\mathbb{R}^{d_1}} p_X(x) \left( \int_{\mathbb{R}^{d_2}} p_{Y|X=x}(y) \log\left(\frac{p_X(x)}{p_{\tilde{X}}(x)}\right) dy \right. \\
&\quad \left. + \int_{\mathbb{R}^{d_2}} p_{Y|X=x}(y) \log\left(\frac{p_{Y|X=x}(y)}{p_{\tilde{Y}|X=x}(y)}\right) dy \right) dx \\
&= \int_{\mathbb{R}^{d_1}} p_X(x) \underbrace{\int_{\mathbb{R}^{d_2}} p_{Y|X=x}(y) dy}_{=1} \log\left(\frac{p_X(x)}{p_{\tilde{X}}(x)}\right) dx \\
&\quad + \int_{\mathbb{R}^{d_1}} p_X(x) \int_{\mathbb{R}^{d_2}} p_{Y|X=x}(y) \log\left(\frac{p_{Y|X=x}(y)}{p_{\tilde{Y}|X=x}(y)}\right) dy dx \\
&= \text{KL}(p_X, p_{\tilde{X}}) + \int_{\mathbb{R}^{d_1}} p_X(x) \text{KL}(p_{Y|X=x}, p_{\tilde{Y}|X=x}) dx \\
&\geq \text{KL}(p_X, p_{\tilde{X}}).
\end{aligned}$$

This proves the claim.  $\square$

The following lemma gives a derivation of the Markov kernel for a general form of the Metropolis-Hastings algorithm. Let  $X'_t$  be a random variable and  $U \sim \mathcal{U}_{[0,1]}$  such that  $(\sigma(X'_t), \sigma(U), \sigma(\cup_{s \leq t-2} \sigma(X_s)))$  are independent. Further, we assume that the joint distribution  $P_{X_{t-1}, X'_t}$  is given by

$$P_{X_{t-1}, X'_t} = P_{X_{t-1}} \times Q_t$$

for some appropriately chosen Markov kernel  $Q_t: \mathbb{R}^d \times \mathcal{B}(\mathbb{R}^d) \rightarrow [0, 1]$ , where  $Q_t(x, \cdot)$  is assumed to have the strictly positive probability density function  $q_t(\cdot|x)$ . We considered the special cases

- MH layer:

$$Q_t(x, \cdot) = \mathcal{N}(x, \sigma^2 I), \quad q(\cdot|x) = \mathcal{N}(\cdot|x, \sigma^2 I).$$

- MALA layer:

$$Q_t(x, \cdot) = \mathcal{N}(x - a_1 \nabla u_t(x), a_2^2 I), \quad q(\cdot|x) = \mathcal{N}(\cdot|x - a_1 \nabla u_t(x), a_2^2 I).$$

Then we have the following lemma, see also [59].

**Lemma B.3.** *Let  $X'_t$  be a random variable such that  $(X_0, \dots, X_{t-1}, X'_t)$  is a Markov chain with Markov kernel  $Q_t := P_{X'_t|X_{t-1}}: \mathbb{R}^d \times \mathcal{B}(\mathbb{R}^d) \rightarrow [0, 1]$ . Assume that  $P_{X'_t|X_{t-1}=x}$  admits a density  $q_t(\cdot|x)$ . Set*

$$\alpha_t(x, y) := \min \left\{ 1, \frac{p_t(y)q_t(y|x)}{p_t(x)q_t(x|y)} \right\}.$$

*Further, let  $U$  be uniformly distributed on  $[0, 1]$  and independent of  $(X_0, \dots, X_{t-1}, X'_t)$ . Then, for  $X_t$  defined by*

$$X_t := 1_{[U,1]}(\alpha_t(X_{t-1}, X'_t)) X'_t + 1_{[0,U[}(\alpha_t(X_{t-1}, X'_t)) X_{t-1},$$

*the transition kernel  $P_{X_t|X_{t-1}}$  is given by*

$$\mathcal{K}_t(x, A) = \int_A q_t(y|x) \alpha_t(x, y) dy + \delta_x(A) \int_{\mathbb{R}^d} q_t(y|x) (1 - \alpha_t(x, y)) dy.$$

*Proof.* For any measurable sets  $A, B \in \mathcal{B}(\mathbb{R}^d)$ , it holds

$$\begin{aligned} P_{X_{t-1}, X_t}(A \times B) &= \int_{\Omega} 1_{\{X_{t-1} \in A\}}(\omega) 1_{\{X_t \in B\}}(\omega) dP(\omega) \\ &= \int_{\Omega} 1_{\{U < \alpha_t(X_{t-1}, X'_t)\}}(\omega) 1_{\{X_{t-1} \in A\}}(\omega) 1_{\{X_t \in B\}}(\omega) dP(\omega) \\ &\quad + \int_{\Omega} 1_{\{U \geq \alpha_t(X_{t-1}, X'_t)\}}(\omega) 1_{\{X_{t-1} \in A\}}(\omega) 1_{\{X_t \in B\}}(\omega) dP(\omega) \end{aligned}$$

Since it holds  $X_t = X'_t$  on  $\{U < \alpha_t(X_{t-1}, X'_t)\}$  and  $X_t = X_{t-1}$  on  $\{U \geq \alpha_t(X_{t-1}, X'_t)\}$ , this is equal to

$$\begin{aligned} & \int_{\Omega} 1_{\{U < \alpha_t(X_{t-1}, X'_t)\}}(\omega) 1_{\{X_{t-1} \in A\}}(\omega) 1_{\{X'_t \in B\}}(\omega) dP(\omega) \\ & + \int_{\Omega} 1_{\{U \geq \alpha_t(X_{t-1}, X'_t)\}}(\omega) 1_{\{X_{t-1} \in A \cap B\}}(\omega) dP(\omega) \\ & = \int_{A \times B \times [0,1]} 1_{[0, \alpha_t(x_{t-1}, x'_t)]}(u) dP_{X_{t-1}, X'_t, U}(x_{t-1}, x'_t, u) \\ & + \int_{(A \cap B) \times \mathbb{R}^d \times [0,1]} 1_{[\alpha_t(x_{t-1}, x'_t), 1]}(u) dP_{X_{t-1}, X'_t, U}(x_{t-1}, x'_t, u). \end{aligned}$$

As  $U$  is independent of  $(X_{t-1}, X'_t)$ , this can be rewritten as

$$\begin{aligned} & \int_{A \times B} \int_{[0,1]} 1_{[0, \alpha_t(x_{t-1}, x'_t)]}(u) dP_U(u) dP_{X_{t-1}, X'_t}(x_{t-1}, x'_t) \\ & + \int_{(A \cap B) \times \mathbb{R}^d} \int_{[0,1]} 1_{[\alpha_t(x_{t-1}, x'_t), 1]}(u) dP_U(u) dP_{X_{t-1}, X'_t}(x_{t-1}, x'_t) \\ & = \int_{A \times B} P_U([0, \alpha_t(x_{t-1}, x'_t)]) dP_{X_{t-1}, X'_t}(x_{t-1}, x'_t) \\ & + \int_{(A \cap B) \times \mathbb{R}^d} P_U([\alpha_t(x_{t-1}, x'_t), 1]) dP_{X_{t-1}, X'_t}(x_{t-1}, x'_t). \end{aligned}$$

Since  $P_U$  is the uniform distribution on  $[0, 1]$ , the above formula becomes

$$\begin{aligned} P_{X_{t-1}, X'_t}(A \times B) &= \int_{A \times B} \alpha_t(x_{t-1}, x'_t) dP_{X_{t-1}, X'_t}(x_{t-1}, x'_t) \\ &+ \int_{(A \cap B) \times \mathbb{R}^d} (1 - \alpha_t(x_{t-1}, x'_t)) dP_{X_{t-1}, X'_t}(x_{t-1}, x'_t) \\ &= \int_{A \times B} \alpha_t(x_{t-1}, x'_t) p_{X_{t-1}, X'_t}(x_{t-1}, x'_t) d(x_{t-1}, x'_t) \\ &+ \int_{(A \cap B) \times \mathbb{R}^d} (1 - \alpha_t(x_{t-1}, x'_t)) p_{X_{t-1}, X'_t}(x_{t-1}, x'_t) d(x_{t-1}, x'_t). \end{aligned}$$

Further, by definition, we have that  $P_{X_{t-1}, X'_t} = P_{X_{t-1}} \times Q_t$  such that  $P_{X_{t-1}, X'_t}$  has the density

$$p_{X_{t-1}, X'_t}(x, y) = q_t(x|y) p_{X_{t-1}}(y).$$

Thus, we get

$$\begin{aligned}
P_{X_{t-1}, X_t}(A \times B) &= \int_A \int_B \alpha_t(x_{t-1}, x'_t) q_t(x'_t | x_{t-1}) dx'_t p_{X_{t-1}}(x_{t-1}) dx_{t-1} \\
&\quad + \int_{A \cap B} \int_{\mathbb{R}^d} (1 - \alpha_t(x_{t-1}, x'_t)) q_t(x'_t | x_{t-1}) dx'_t p_{X_{t-1}}(x_{t-1}) dx_{t-1} \\
&= \int_A \int_B \alpha_t(x_{t-1}, x'_t) q_t(x'_t | x_{t-1}) dx'_t dP_{X_{t-1}}(x_{t-1}) \\
&\quad + \int_A \delta_{x_{t-1}}(B) \int_{\mathbb{R}^d} (1 - \alpha_t(x_{t-1}, x'_t)) q_t(x'_t | x_{t-1}) dx'_t dP_{X_{t-1}}(x_{t-1}) \\
&= \int_A \left( \int_B \alpha_t(x_{t-1}, x'_t) q_t(x'_t | x_{t-1}) dx'_t \right. \\
&\quad \left. + \delta_{x_{t-1}}(B) \int_{\mathbb{R}^d} (1 - \alpha_t(x_{t-1}, x'_t)) q_t(x'_t | x_{t-1}) dx'_t \right) dP_{X_{t-1}}(x_{t-1}) \\
&= \int_A \mathcal{K}_t(x_{t-1}, B) dP_{X_{t-1}}(x_{t-1}).
\end{aligned}$$

In summary, we obtain

$$P_{X_{t-1}, X_t}(A \times B) = \int_A \mathcal{K}_t(x_{t-1}, B) dP_{X_{t-1}}(x_{t-1}).$$

As the measurable rectangles are a  $\cap$ -stable generator of  $\mathcal{B}(\mathbb{R}^d \times \mathbb{R}^d)$ , this yields that  $P_{X_{t-1}, X_t} = P_{X_{t-1}} \times \mathcal{K}_t$  such that  $P_{X_t | X_{t-1}} = \mathcal{K}_t$ .  $\square$

## Acknowledgements

The funding by the German Research Foundation (DFG) within the projects STE 571/16-1 and within the project of the DFG-SPP 2298 „Theoretical Foundations of Deep Learning“ is gratefully acknowledged. Many thanks to S. Heidenreich from the Physikalisch-Technische Bundesanstalt (PTB) for providing the scatterometry data which we used for training the forward model and for fruitful discussions on the corresponding example. P. H. thanks J. Köhler for helpful discussions. We would like to thank A. Houdard for generating the image on the bottom of Figure 2.3. Many thanks to V. Stein for proofreading.

## References

- [1] B. D. Anderson. Reverse-time diffusion equation models. *Stochastic Processes and their Applications*, 12(3):313–326, 1982.
- [2] A. Andrle, N. Farchmin, P. Hagemann, S. Heidenreich, V. Soltwisch, and G. Steidl. Invertible neural networks versus MCMC for posterior reconstruction in grazing incidence X-ray fluorescence. In A. Elmoataz, J. Fadili, Y. Quéau, J. Rabin, and L. Simon, editors, *Scale Space and Variational Methods*, volume 12679 of *Lecture Notes in Computer Science*, pages 528–539. Springer, 2021.

- [3] M. Arbel, A. Matthews, and A. Doucet. Annealed flow transport monte carlo. *ArXiv 2102.07501*, 2021.
- [4] L. Ardizzone, J. Kruse, C. Rother, and U. Köthe. Analyzing inverse problems with invertible neural networks. In *7th International Conference on Learning Representations, ICLR 2019, New Orleans, LA, USA, May 6-9, 2019*, 2019.
- [5] L. Ardizzone, C. Lüth, J. Kruse, C. Rother, and U. Köthe. Guided image generation with conditional invertible neural networks. *ArXiv 1907.02392*, 2019.
- [6] J. Behrmann, W. Grathwohl, R. Chen, D. Duvenaud, and J.-H. Jacobsen. Invertible residual networks. In *International Conference on Machine Learning*, pages 573–582, 2019.
- [7] J. Behrmann, P. Vicol, K.-C. Wang, R. Grosse, and J.-H. Jacobsen. Understanding and mitigating exploding inverses in invertible neural networks. *ArXiv 2006.09347*, 2020.
- [8] R. Chen, J. Behrmann, D. K. Duvenaud, and J.-H. Jacobsen. Residual flows for invertible generative modeling. In *Advances in Neural Information Processing Systems*, volume 32. Curran Associates, Inc., 2019.
- [9] P. L. Combettes and J.-C. Pesquet. Deep neural network structures solving variational inequalities. *Set-Valued and Variational Analysis*, pages 1–28, 2020.
- [10] R. Cornish, A. L. Caterini, G. Deligiannidis, and A. Doucet. Relaxing bijectivity constraints with continuously indexed normalising flows. *ArXiv 1909.13833*, 2019.
- [11] E. Cunningham, R. Zabounidis, A. Agrawal, I. Fiterau, and D. Sheldon. Normalizing flows across dimensions. *ArXiv 2006.13070*, 2020.
- [12] B. Dai and D. P. Wipf. Diagnosing and enhancing VAE models. In *International Conference on Learning Representations*, 2019.
- [13] N. De Cao, I. Titov, and W. Aziz. Block neural autoregressive flow. *ArXiv 1904.04676*, 2019.
- [14] A. Denker, M. Schmidt, J. Leuschner, and P. Maass. Conditional invertible neural networks for medical imaging. *Journal of Imaging*, 7(11):243, 2021.
- [15] L. Dinh, J. Sohl-Dickstein, and S. Bengio. Density estimation using real NVP. In *5th International Conference on Learning Representations, ICLR 2017, Toulon, France, April 24-26, 2017, Conference Track Proceedings*, 2017.
- [16] C. Durkan, A. Bekasov, I. Murray, and G. Papamakarios. Neural spline flows. *Advances in Neural Information Processing Systems*, 2019.
- [17] C. Durkan and Y. Song. On maximum likelihood training of score-based generative models. *ArXiv 2101.09258*, 2021.
- [18] L. Falorsi, P. de Haan, T. R. Davidson, W. De Cao, N., P. M., Forr'e, and T. S. Cohen. Explorations in homeomorphic variational auto-encoding. *ArXiv 807.04689*, 2018.

- [19] L. Falorsi, P. de Haan, T. R. Davidson, and P. Forré. Reparameterizing distributions on Lie groups. *ArXiv 1903.02958*, 2019.
- [20] M. Girolami and B. Calderhead. Riemann manifold Langevin and Hamiltonian Monte Carlo methods. *J. R. Stat. Soc.: Series B (Statistical Methodology)*, 73(2):123–214, 2011.
- [21] M. González, A. Almansa, and P. Tan. Solving inverse problems by joint posterior maximization with autoencoding prior. *ArXiv 2103.01648*, 2021.
- [22] I. Goodfellow, Y. Bengio, and A. Courville. *Deep learning*. MIT press, 2016.
- [23] A. A. Gritsenko, J. Snoek, and T. Salimans. On the relationship between normalising flows and variational- and denoising autoencoders. In *Deep Generative Models for Highly Structured Data, ICLR 2019 Workshop*, 2019.
- [24] P. Hagemann, J. Hertrich, and G. Steidl. Stochastic normalizing flows for inverse problems: a Markov Chains viewpoint. *ArXiv 2109.11375*, 2021.
- [25] P. L. Hagemann and S. Neumayer. Stabilizing invertible neural networks using mixture models. *Inverse Problems*, 2021.
- [26] M. Hasannasab, J. Hertrich, S. Neumayer, G. Plonka, S. Setzer, and G. Steidl. Parseval proximal neural networks. *J. Fourier Anal. Appl.*, 26:59, 2020.
- [27] U. G. Haussmann and E. Pardoux. Time reversal of diffusions. *The Annals of Probability*, pages 1188–1205, 1986.
- [28] K. He, X. Zhang, S. Ren, and J. Sun. Deep residual learning for image recognition. In *Proceedings of the IEEE Conference on Computer Vision and Pattern Recognition*, pages 770–778, 2016.
- [29] S. Heidenreich, H. Gross, and M. Bär. Bayesian approach to the statistical inverse problem of scatterometry: Comparison of three surrogate models. *Int. J. Uncertain. Quantif.*, 5(6), 2015.
- [30] S. Heidenreich, H. Gross, and M. Bär. Bayesian approach to determine critical dimensions from scatterometric measurements. *Metrologia*, 55(6):S201, Dec. 2018.
- [31] J. Hertrich, A. Houdard, and C. Redenbach. Wasserstein patch prior for image superresolution. *ArXiv 2109.12880*, 2021.
- [32] J. Hertrich, S. Neumayer, and G. Steidl. Convolutional proximal neural networks and plug-and-play algorithms. *Linear Algebra and its Applications*, 631:203–234, 2020.
- [33] A. Houdard, A. Leclaire, N. Papadakis, and J. Rabin. Wasserstein generative models for patch-based texture synthesis. In A. Elmoataz, J. Fadili, Y. Quéau, J. Rabin, and L. Simon, editors, *Scale Space and Variational Methods in Computer Vision*, page 269–280, Cham, 2021. Springer International Publishing.

- [34] C.-W. Huang, D. Krueger, A. Lacoste, and A. Courville. Neural autoregressive flows. In *Proc. of the 35th International Conference on Machine Learning*, pages 2078–2087. PMLR, 2018.
- [35] A. Hyvärinen and P. Dayan. Estimation of non-normalized statistical models by score matching. *Journal of Machine Learning Research*, 6(4), 2005.
- [36] P. Jaini, I. Kobyzhev, Y. Yu, and M. Brubaker. Tails of lipschitz triangular flows. *ArXiv 1907.04481*, 2019.
- [37] D. P. Kingma and P. Dhariwal. Glow: Generative flow with invertible 1x1 convolutions. *ArXiv 1807.03039*, 2018.
- [38] D. P. Kingma and M. Welling. Auto-encoding variational bayes. *ArXiv 1312.6114*, 2013.
- [39] D. P. Kingma and M. Welling. An introduction to variational autoencoders. *Foundations and Trends in Machine Learning*, 12(4):307–392, 2019.
- [40] K. Kothari, A. Khorashadizadeh, M. de Hoop, and I. Dokmanić. Trumpets: Injective flows for inference and inverse problems. *ArXiv 2102.10461*, 2021.
- [41] J.-F. Le Gall. *Brownian motion, martingales, and stochastic calculus*, volume 274 of *Graduate Texts in Mathematics*. Springer, [Cham], 2016.
- [42] C. Louizos and M. Welling. Multiplicative normalizing flows for variational Bayesian neural networks. In *Proc. of the 34th International Conference on Machine Learning*, pages 2218–2227. PMLR, 2017.
- [43] M. Mirza and S. Osindero. Conditional generative adversarial nets. *ArXiv 1411.1784*, 2014.
- [44] T. Müller, McWilliams, R. B., M. F., Gross, and J. Novák. Neural importance sampling. *ArXiv 1808.03856*, 2018.
- [45] D. Nielsen, P. Jaini, E. Hoogeboom, O. Winther, and M. Welling. SurVAE Flows: surjections to bridge the gap between VAEs and flows. *NeurIPS*, 2020.
- [46] J. P. Nilmeier, C. G. E., M. D. D. L., and C. J.D. Nonequilibrium candidate monte carlo is an efficient tool for equilibrium simulation. *Proc. Natl. Acad. Sci. USA*, 108:1009–1018, 2011.
- [47] G. Papamakarios, T. Pavlakou, , and I. Murray. Masked autoregressive flow for density estimation. *Advances in Neural Information Processing Systems*, page 2338–2347, 2017.
- [48] J.-C. Pesquet, A. Repetti, M. Terris, and Y. Wiaux. Learning maximally monotone operators for image recovery. *SIAM Journal on Imaging Sciences*, 14(3):1206–1237, 2021.
- [49] D. Rezende and S. Mohamed. Variational inference with normalizing flows. In F. Bach and D. Blei, editors, *Proceedings of the 32nd International Conference on Machine Learning*, volume 37 of *Proceedings of Machine Learning Research*, pages 1530–1538, Lille, France, 07–09 Jul 2015. PMLR.

[50] D. J. Rezende and S. Mohamed. Variational inference with normalizing flows. *ArXiv 1505.05770*, 2015.

[51] G. O. Roberts and J. S. Rosenthal. General state space Markov chains and MCMC algorithms. *Probability Surveys*, 1:20 – 71, 2004.

[52] G. O. Roberts and R. L. Tweedie. Exponential convergence of Langevin distributions and their discrete approximations. *Bernoulli*, 2(4):341–363, 1996.

[53] L. Ruthotto and E. Haber. An introduction to deep generative modeling. *DMV Mitteilungen*, 44(3):1–24, 2021.

[54] J. Sohl-Dickstein, E. A. Weiss, N. Maheswaranathan, and S. Ganguli. Deep unsupervised learning using nonequilibrium thermodynamics. *ArXiv 1503.03585*, 2015.

[55] K. Sohn, H. Lee, and X. Yan. Learning structured output representation using deep conditional generative models. *Advances in neural information processing systems*, 28:3483–3491, 2015.

[56] Y. Song and S. Ermon. Generative modeling by estimating gradients of the data distribution. *ArXiv 1907.05600*, 2019.

[57] Y. Song, J. Sohl-Dickstein, D. P. Kingma, A. Kumar, S. Ermon, and B. Poole. Score-based generative modeling through stochastic differential equations. *ArXiv 2011.13456*, 2020.

[58] T. Teuber, G. Steidl, P. Gwosdek, C. Schmaltz, and J. Weickert. Dithering by differences of convex functions. *SIAM Journal on Imaging Science*, 4(1):79–108, 2011.

[59] L. Tierney. A note on Metropolis-Hastings kernels for general state spaces. *Annals of Applied Probability*, 8(1):1–9, 1998.

[60] D. Tsvetkov, L. Hristov, and R. Angelova-Slavova. On the convergence of the Metropolis-Hastings Markov chains. *ArXiv 1302.0654v4*, 2020.

[61] A. Vahdat, K. Kreis, and J. Kautz. Score-based generative modeling in latent space. *ArXiv 2106.05931*, 2021.

[62] M. Welling and Y.-W. Teh. Bayesian learning via stochastic gradient Langevin dynamics. In *International Conference on Machine Learning*, page 681–688, 2011.

[63] C. Winkler, D. Worrall, E. Hoogeboom, and M. Welling. Learning likelihoods with conditional normalizing flows. *ArXiv 1912.00042*, 2019.

[64] H. Wu, J. Köhler, and F. Noé. Stochastic normalizing flows. In H. Larochelle, M. A. Ranzato, R. Hadsell, M. Balcan, and H. Lin, editors, *Advances in Neural Information Processing Systems 2020*, 2020.

[65] Q. Zhang and Y. Chen. Diffusion normalizing flow. In *Conference on Neural Information Processing Systems*, 2021.